HHS Public Access

Author manuscript

Dev Cell. Author manuscript; available in PMC 2020 December 16.

Published in final edited form as:

Dev Cell. 2019 December 16; 51(6): 759–774.e5. doi:10.1016/j.devcel.2019.11.005.

Primary cilia signaling promotes axonal tract development and is disrupted in Joubert Syndrome Related Disorder models

Jiami Guo[1,2,*], **James Otis**[1,^], **Sarah K. Suciu**[3,^], **Christy Catalano**[2,^], **Lei Xing**[1], **Sandii Constable**[3], **Dagmar Wachten**[4], **Stephanie Gupton**[1], **Janice Lee**[1], **Amelia Lee**[1], **Katherine H. Blackley**[1], **Travis Ptacek**[1], **Jeremy M. Simon**[1], **Stephane Schurmans**[5], **Garret D. Stuber**[6], **Tamara Caspary**[3,*], **E. S. Anton**[1,*]

[1]UNC Neuroscience Center and the Department of Cell and Molecular Physiology, University of North Carolina School of Medicine, Chapel Hill, NC 27599

[2]Hotchkiss Brain Institute and the Department of Cell Biology and Anatomy, University of Calgary, Calgary, AB T2N 4N1

[3]Department of Human Genetics, Emory University School of Medicine, Atlanta, GA 30322

[4]Biophysical Imaging, Institute of Innate Immunity, University Hospital Bonn, University of Bonn, Germany

[5]Laboratory of Functional Genetics, GIGA Research Center, University of Liège, Belgium

[6]Center for the Neurobiology of Addiction, Pain, and Emotion, Department of Anesthesiology and Pain Medicine, University of Washington, Seattle, WA 98195

Summary

Appropriate axonal growth and connectivity are essential for functional wiring of the brain. Joubert Syndrome Related disorders (JSRD), a group of ciliopathies in which mutations disrupt primary cilia function, are characterized by axonal tract malformations. However, little is known about how cilia-driven signaling regulates axonal growth and connectivity. We demonstrate that the deletion of related JSRD genes, *Arl13b* and *Inpp5e,* in projection neurons leads to de-fasciculated and mis-oriented axonal tracts. *Arl13b* deletion disrupts the function of its downstream effector Inpp5e and deregulates ciliary-PI3K/AKT signaling. Chemogenetic activation of ciliary-GPCR signaling and cilia-specific optogenetic modulation of downstream second messenger cascades (PI3K, AKT, AC3) commonly regulated by ciliary signaling receptors induce rapid changes in axonal dynamics. Further, *Arl13b* deletion leads to changes in

[*]Corresponding authors (jiami.guo@ucalgary.ca, tcaspar@emory.edu, anton@med.unc.edu).
[^]Equal contributors
Lead Contact: E. S. Anton, anton@med.unc.edu, PHONE: 919-843-6114

Author Contributions

JG, TC, and EA designed the experiments and supervised the project. JG, JO, CC, LX, DW, SKS, SG, SC, AL, JL, KHB, TP, JMS, GDS, TC, and EA conducted the experiments and analyzed the data. JG, DW, GDS, SG, TC, and EA wrote the manuscript.

Declaration of competing financial interests

The authors declare no competing interests.

transcriptional landscape associated with dysregulated PI3K/AKT signaling. These data suggest that ciliary signaling acts to modulate axonal connectivity and that impaired primary cilia signaling underlies axonal tract defects in JSRD.

eTOC Blurb

Guo et al. show that primary cilia-driven signaling regulates growth cone dynamics and axonal tract development. Ciliary signaling receptor activation and associated changes in signaling cascades (PI3K, AKT, AC3) and transcriptional landscape affect axons. Disrupted ciliary signaling following mutations in Arl13b or Inpp5e lead to axonal tract malformations in JSRD.

Graphical Abstract

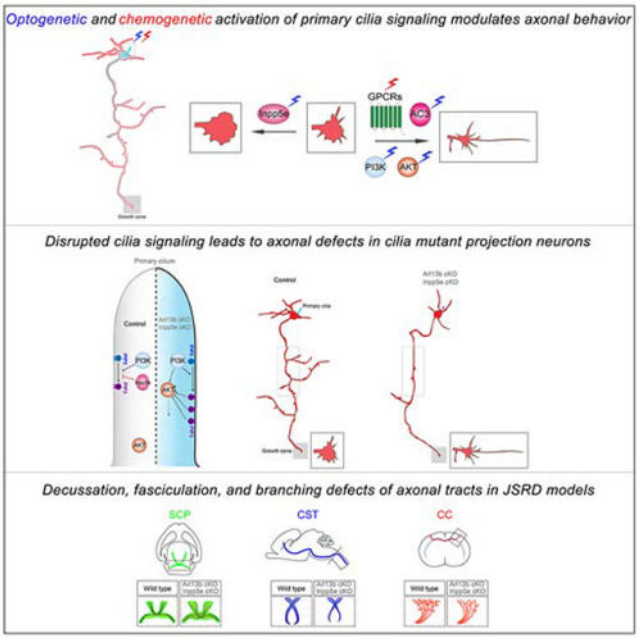

Keywords

Primary cilia; axonal pathways; ciliopathies; connectome; brain development; molar tooth sign; Joubert Syndrome Related Disorders

Introduction

Primary cilia are present on virtually all cell types and, when defective, can lead to ciliopathies, occurring on the order of ~1:10,000 live births in the general population. A diagnostic feature of many ciliopathies is axonal tract defects (Green et al., 2018; Guadiana et al., 2013; Guemez-Gamboa et al., 2014; Hildebrandt et al., 2011; Reiter and Leroux, 2017; Sarkisian and Guadiana, 2015; Parisi, 2019; Poretti et al., 2007). Appropriate axonal growth and pathfinding are essential for wiring the developing brain (Chedotal and Richards, 2010; Engle, 2010). Axonal tract phenotypes in ciliopathies imply a role for primary cilia in

axonal development and connectivity, but it is unclear how cilia-driven signaling emanating from near the neuronal soma acts to regulate axonal growth and connectivity.

Joubert Syndrome Related disorders (JSRD), a prominent collection of ciliopathies, are autosomal recessive, congenital disorders with a variety of neurological symptoms including developmental delay, intellectual disabilities (ID), abnormal respiratory rhythms, hypotonia, ataxia, oculomotor apraxia, and mirror movement synkinesis (Parisi, 2019). The diagnostic feature of JSRD is the axonal tract malformation called the molar tooth sign (MTS), which presents as thickened, elongated, and horizontally orientated superior cerebellar peduncles (SCPs) that fail to decussate in the midbrain (Brancati et al., 2010; Juric-Sekhar et al., 2012; Parisi, 2019; Romani et al., 2013; Sattar and Gleeson, 2011; Senocak et al., 2010). In addition to SCP malformation, absent or reduced decussation of the corticospinal tract (CST), corpus callosum (CC), and central pontine tracts are frequently observed in JSRD patients. Consistent with these axonal anomalies and the resultant changes in brain wiring, JSRD patients are often diagnosed with intellectual disabilities and autism spectrum disorder (ASD) (Marley and von Zastrow, 2012; Novarino et al., 2011; Reiter and Leroux, 2017).

Causative mutations for JSRD have been identified in 30+ cilia-related genes (Reiter and Leroux, 2017), implying a role for primary cilia in axon growth and guidance. To understand the role of primary cilia in axonal development and connectivity in the context of JSRD, we examined the function of two interrelated JSRD genes *ARL13B* (*JBTS8*, a small GTPase) and *INPP5E* (*JBTS1*, a phosphoinositide 5-phosphatase), respectively, in axonal development. ARL13B complexes with INPP5E, localize to primary cilia and both are essential for ciliary function. ARL13B is known for regulating ciliary signaling receptor (e.g., GPCRs, PDGFRα, Smo) localization, whereas INPP5E controls the phosphoinositide composition of ciliary membrane and thus receptor trafficking, localization, and downstream signaling cascade activation (e.g. PI3K/AKT) (Barral et al., 2012; Bielas et al., 2009; Cantagrel et al., 2008; Caspary et al., 2007; Garcia-Gonzalo et al., 2015; Mariani et al., 2016; Nachury et al., 2010; Phua et al., 2017; Umberger and Caspary, 2015). Deletion of *Arl13b* or *Inpp5e* impairs the ability of the primary cilium to function as a signaling hub, thus providing excellent molecular models to examine how cilia driven signaling regulate axon growth and connectivity in normal and JSRD brains.

Here, using neuron specific mouse genetic models of *Arl13b* and *Inpp5e*, related human mutations, and chemo-genetic and opto-genetic manipulation of primary cilia signaling, we demonstrate that ciliary signaling lies at the heart of appropriate patterns of axon tract development and connectivity.

Results

Aberrant axonal pathway development in *Arl13b* mutants

To evaluate the effect of primary cilia in axonal development, *Nex-Cre* line was used to delete *Arl13b* in post mitotic cortical projection and deep cerebellar neurons (Goebbels et al., 2006; Su et al., 2012). These projection neurons are ciliated (SFig.1). The Nex-Cre line enables Cre recombinase-mediated deletion of *Arl13b* allele in these neurons from E13.5 (Higginbotham et al., 2012). Cre-dependent Tau^{mGFP} or *Ai9* reporter lines were used to

visualize axons with GFP or mRFP, respectively (Hippenmeyer et al., 2005; Madisen et al., 2010). Deletion of Arl13b did not affect the survival of cortical projection or deep cerebellar neurons (SFig.2).

SCP axons of the deep cerebellar nuclei (DCN) extend toward and decussate in the caudal half of the midbrain, pass below and lateral to the red nucleus in the rostral midbrain, innervate the red nucleus, and then extend rostrally to the ventrolateral nucleus (VLN) of the thalamus (Fig.1A–B). The initial outgrowth of SCP from cerebellum is diffuse in Arl13b mutants (*Arl13b*$^{lox/lox}$*; Nex-Cre; Tau*^{mGFP}) (SFig.3A–D). Decussating SCP axons exiting cerebellum in controls (*Arl13b* $^{lox/+}$*; NexCre; Tau*^{mGFP}) turn rostrally at 91±2.4° angle, whereas in mutants, SCP turns with a significantly wider angle (118±2.8°; SFig.3E–F), suggesting a less coalesced and horizontally oriented SCP projection. The decussating Arl13b-deficient SCP axonal bundles are wider, loosely fasciculated, and contain misoriented fibers (Fig.1C–F; SCP Width [axial]: Control, 291±17μm, Arl13b cKO, 355±12μm; n=6 brains per group). To examine the projection pattern of SCP, AAV5-Synapsin-tdTomato virus (Klapoetke et al., 2014) was unilaterally injected into the DCN of control and *Arl13b-NexCre* mutant mice to label DCN axons (Fig.1B, G, H, O). Compared to control, the decussation of mutant SCP is wider (Fig.1I, J, P) and the DCN axonal projection into RN (Fig.1K, K', L, L', Q) and VLN is significantly reduced (Fig.1M, N, R).

To examine other JSRD relevant axonal tracts disrupted in Arl13b mutants, we analyzed the corticospinal tract (CST). At P1, pyramidal decussation of CST is markedly disrupted (Fig. 2A–E). Clearly decussating pyramidal axons were evident in control (Fig. 2B, D, arrowheads), but were significantly reduced in *Arl13b*$^{lox/lox}$*; NexCre* brains (Fig. 2C, E, arrows). Consistent with this, the density of axons, post decussation, innervating the distal cervical spinal cord, is reduced in *Arl13b-NexCre* mutants (Fig.2F [arrowhead], G [arrow]). Together, these results suggest that the NexCre deletion of *Arl13b* in postmitotic cortical neurons leads to disrupted CST formation and decussation.

To assess the effect of Arl13b deletion in callosal projection neurons, we performed unilateral in utero electroporation (IUE) at E15.5 with CAG-Cre and CAG-EGFP plasmids leading to *Arl13b* deletion and GFP labeling of callosally projecting neurons of layers 2/3 (Fig.2H). Callosal axons were analyzed at P1, as they cross the cortical midline to form the corpus callosum (CC) (Fig.2I–J). Compared to controls, Arl13b-deficient axons are loosely organized, poorly fasciculated, and form a wider CC tract (Fig.2I, I', J, J'; midline width of CC tract: control (95.2±1.2μm), mutant (140.2±4.4μm), Student's *t*-test, p =6.2E-5, n=4 brains). The midline crossing growth cones of Arl13b-deficient neurons also display longer filopodial projections compared to control neurons (Fig.2I", J"[arrowhead]); mutant: 5.63±0.22μm, control: 2.31±0.27μm, Student's *t*-test, p =0.001, n=16 neurons). At P21, as CC axons reach their targets, control CC axons extensively branch and innervate ipsilateral layer 5 and contralateral layers 2/3 and 5 (Fig.2M, O[asterisk]). In contrast, Arl13b-deficient CC displayed dis-organized axons (Fig.2K–L), as well as reduced axonal branching and innervation of target layers (Fig.2N[asterisk], P[asterisk], Q, R). Lastly, decussation defects were also evident in the pontine nuclei. Transverse pontine tegmental axons do not decussate normally and are misoriented (SFig.3G–H).

Thickened superior cerebellar peduncles that show disorganized decussation, perturbed pyramidal axon decussation, and transverse pontine fiber defects are consistent with the axonal phenotypes seen in JSRD. Our observations suggest that *Arl13b* deletion in projection neurons disrupts axonal tract development in a manner consistent with human JSRD phenotype. Further, these results suggest that disruption of primary cilia signaling through the deletion of *Arl13b* disrupts the appropriate formation and connectivity of major axon tracts in the brain, including SCP, CST, and CC. We therefore sought to explore the relationship between cilia signaling and axonal development.

Deletion of *Arl13b* leads to altered axon growth behavior

To examine developmental changes in patterns of axon growth in Arl13b-deficient neurons, we isolated and cultured Ai9^{+} DCN neurons from control and *Arl13b$^{lox/lox}$; Nex-Cre; Ai9* (Arl13b cKO) brains. Evaluation of different stages of neuronal polarization (Banker, 2018) after initial plating suggests that axon-dendritic polarization (SFig.4) or axon formation and outgrowth are not affected in the absence of Arl13b, but fewer and shorter lateral axonal branches were seen in Arl13b-deficient neurons (Fig.3A [arrowheads], B–C). Live imaging indicates that control axonal branches arise along the main axonal shaft (Fig.3D [arrowheads], E). Consistent with the reduced axonal branching observed, mutant DCN neuron axons showed significantly reduced formation and dynamics of axonal branching protrusions (Fig.3D–E). These results suggest defects in the initiation and extension of axonal branching in Arl13b-deficient neurons.

We also observed reduced dendritic outgrowth of mutant DCN neurons in vitro (Fig.3A; total dendritic length $_{[DIV3]}$: control (274.1±12.9μm), mutant (116.5±10.0μm), Student's *t*-test, p=2.34E-11; # of primary dendrites$_{[DIV3]}$: control (5.7±0.3), mutant (3.1±0.2), Student's *t*-test, p=2.58E-08, n =16 $_{[Control]}$, 17 $_{[mutant]}$ neurons).

Compared to control DCN neuron growth cones that show characteristic lamellipodial veils in between dynamic filopodial extensions ($t_{1/2}$ [half lifetime]=24.4± 1.3s), Arl13b-deficient growth cones are smaller but have numerous longer filopodial protrusions (Fig.3F–G [arrowheads]) with significantly reduced dynamics ($t_{1/2}$=118.5± 3.3s, Student's *t*-test, p<0.05, n=12 cells). Further, Arl13b null (Arl13b$^{-/-}$) embryonic cortical neurons also show reduced axon branching and disrupted growth cone morphology (SFig.5). Axons of Ift88 null (Ift88$^{-/-}$) cortical neurons without primary cilia were similarly affected (SFig.5). Together, these *in vitro* observations suggest that in the absence of appropriate primary cilia signalling, axonal growth cone dynamics and the filopodia to lamellipodia balance are altered.

The fasciculation defects *in vivo* and the axonal branching and growth cone defects *in vitro* in Arl13b-deficient axons suggest that communication and interactions between axons as they branch and extend as fiber tracts may have been perturbed in cilia mutant neurons. Intercellular recognition through adhesion molecules such as protocadherins are essential for axon growth and fasciculation. Within the protocadherin family, Protocadherin-17 (Pcdh17) is highly expressed in cortical and DCN neurons. Recruitment of Pcdh17 to axon-axon contacts is thought to facilitate the fasciculation and collective extension of the developing SCP axons (Hayashi et al., 2014; Hoshina et al., 2013). We therefore examined if primary

cilia signaling is necessary to recruit Pcdh17 to points of axonal contacts *in vitro*. Control or Arl13b-deficient cortical neurons labeled with either BFP or tdTomato/Pcdh17-EGFP were plated onto different sides of microfluidic chambers, allowing for the establishment of direct axon-axon contacts between BFP^+ and $tdTom^+$ neurons (Fig.3H). Compared to control neurons that show expression of Pcdh17 at axonal points of contacts, Arl13b-deficient neurons show reduced recruitment of Pcdh17 to axon-axon contacts (Fig.3I–K). These observations suggest that disrupted ciliary signaling in Arl13b-deficient neurons can impair axon-axon recognition/ adhesion signals necessary for the organized growth of axonal tracts.

Multiple mutations (p. R79Q, p. W82X, p. Y86C, p. R200C, p. G75R) in ARL13B are known to cause JSRD (Cantagrel et al., 2008; Juric-Sekhar et al., 2012; Miertzschke et al., 2014; Parisi, 2019; Rafiullah et al., 2017; Thomas et al., 2015). To test whether these JSRD mutant alleles affect axonal growth, we cre-inducibly expressed them in Arl13b-deficient DCN neurons (Guo et al., 2017). Wild-type human ARL13B rescued the branching defects in the Arl13b-deficient DCN neurons (Fig. 3L–M). However, JSRD causing variants R79Q, G75R, W82X, Y86C, and R200C failed to do so consistent with their known disruption of Inpp5e ciliary targeting (Fig.3L–M; (Humbert et al., 2012). These results suggest that human mutations in Arl13b disrupt axonal development. Further, a mouse nonciliary form of functional Arl13b (V358A; Higginbotham et al., 2012) also did not rescue the axonal branching defects in Arl13b-deficient DCN neurons (Fig.3L–M), suggesting that the localization and activity of Arl13b within the primary cilium is crucial to its role in the appropriate regulation of axonal growth pattern.

Collectively, these observations reveal that neurons deficient in ciliary Arl13b display reduced axonal branching, aberrant growth cone morphology, altered filopodia/lamellipodial balance, and impaired axon-axon adhesive contacts.

Arl13b-Inpp5e pathway

To define the signaling mechanisms underlying Arl13b mediated axonal dynamics, we first examined inositol polyphosphate-5-phosphatase (Inpp5e*)* as Inpp5e is absent in *Arl13b*-deficient cilia indicating Arl13b is necessary for Inpp5e ciliary targeting (Humbert et al., 2012). Inpp5e hydrolyzes the 5-phosphate of PtdIns(4,5)P2 and PtdIns(3,4,5)P3 (PIP2 and PIP3), which act as docking phospholipids necessary for ciliary localization of signaling receptors and activation of signaling cascades. Importantly, mutations in *INPP5E* lead to JSRD and axonal tract defects (Bielas et al., 2009; Conduit et al., 2012; Garcia-Gonzalo et al., 2015; Jacoby et al., 2009). These observations suggest that Inpp5e acts as an effector of Arl13b. The deficiency of ciliary Inpp5e, due to either deletion of *Arl13b* or *Inpp5e*, may compromise the Arl13b-Inpp5e signaling pathway necessary for axonal tract development.

We therefore examined SCP, CST, and CC tract formation and organization in *Inpp5e-NexCre* (Inpp5e cKO*)* brains. Similar to *Arl13b-NexCre* mutants, *Inpp5e-NexCre* mutant SCP tracts are diffuse, wider, and loosely fasciculated (Fig. 4A–D; SCP Width (axial): Control, 285±19μm, Inpp5e cKO, 349±23μm; $P<0.05$ (Student's *t*-test); n=6 brains per group). Mutant CST tract displays reduced pyramidal decussation (Fig.4E–G). Inpp5e-deficient callosal axons show significantly reduced branching and target innervation when compared to controls (Fig.4H–M). Further, reduced axonal branching and aberrant growth

cone morphology similar to that of Arl13b-deficient neurons were seen Inpp5e-deficient DCN neurons *in vitro* (Fig.4N–Q). Reduced dendritic growth is also evident in Inpp5e mutant DCN neurons *in vitro* (Fig. 4N; total dendritic length $_{[DIV3]}$: control (292.1±23.4μm), mutant (101.5±8.3μm), Student's *t*-test, p=1.28E-13; # of primary dendrites$_{[DIV3]}$: control (5.3±0.6), mutant (2.9±0.2), Student's *t*-test, p=1.52E-09, n=16 neurons).

These common defects in Arl13b and Inpp5e-deficient neurons suggest that both can regulate neuronal development from the cilium. We therefore set out to delineate the Arl13b-Inpp5e regulated signaling mechanisms, which when perturbed in cilia, could affect axonal development.

Arl13b-Inpp5e pathway converges on ciliary-PI3K/AKT signaling

PI(4,5)P2 and PI(3,4,5)P3, the main substrates of Inpp5e downstream of Arl13b, are major second messengers of receptor tyrosine kinases (RTK), GPCR, and Shh pathways (Bielas et al., 2009; Conduit et al., 2012; Garcia-Gonzalo et al., 2015; Oude Weernink et al., 2007; Phua et al., 2017). Several RTKs, GPCRs and Smo receptors selectively accumulate in neuronal primary cilia (Christensen et al., 2012; Hilgendorf et al., 2016; Reiter and Leroux, 2017). Upon activation, GPCR, Shh and RTK signaling lead to the activation of phosphatidylinositol 3-kinase (PI3K) and the production of PIP3, which in turn activates AKT to orchestrate a broad spectrum of cellular functions, including axonal outgrowth and growth cone dynamics (Hakim et al., 2012; Henle et al., 2011; Manning and Cantley, 2007; Manning and Toker, 2017; Oude Weernink et al., 2007). Consistent with the role of Inpp5e that hydrolyzes PIP3, deletion of Inpp5e leads to enrichment of PIP3 at primary cilia and elevated whole cell PI3K-AKT signaling activity (Dyson et al., 2017; Phua et al., 2017; Plotnikova et al., 2015). To test the hypothesis that ciliary Arl13b-Inpp5e signaling converges onto the production of ciliary PIP3 and activation of AKT to regulate axonal development, we first examined the level of PIP3 in Arl13b and Inpp5e-deficient neuronal cilia. We expressed PIP3 biosensors RFP-PH$_{AKT}$ or mCh-PH$_{GRPI}$ in DCN neurons from control, Arl13b cKO, and Inpp5e cKO brains (Idevall-Hagren et al., 2012). Compared to control, a significant increase in the levels of PIP3 was observed in Arl13b and Inpp5e-deficient neuronal primary cilia (SFig. 6A–E). We found a similar increase of PIP3 level in *Arl13b* null cortical neurons (SFig. 6F–K). These observations suggest that deletion of *Arl13b* or *Inpp5e* leads to increased ciliary PIP3. To test whether the increased PIP3 levels lead to elevated activity of AKT, we examined the phosphorylation level of AKT, and its downstream effectors glycogen synthase kinase 3 (GSK3), ribosomal protein S6 kinase (S6K), and transcription factor cyclic AMP-response element binding protein (CREB), in control and Arl13b null or Inpp5e deficient (*Inpp5e*^{rdg}; Su et al., 2012) brains. A significant increase of p-AKT, p-GSK, p-S6, and p-CREB is evident in both Arl13b and Inpp5e deficient brains (SFig. 6L–M), suggesting an elevated global level of AKT activity follows the loss of Arl13b or Inpp5e. Taken together, these results reveal that deficiency of Arl13b-Inpp5e in neurons lead to increased levels of ciliary PIP3 as well as elevated global AKT activity.

Optogenetic/Chemogenetic manipulations of ciliary-GPCR and ciliary-PI3K/AKT signaling change axonal behavior

We therefore set out to further delineate the role of cilia-regulated PI3K/AKT pathway on axonal development. First, to evaluate the effect of acute activation of ciliary signaling receptors upstream of PI3K on axons, we focused on ciliary-GPCR signaling that can activate the PI3K signaling pathway (Fig.5A; Spangler and Bruchas, 2017). We employed a chemogenetic approach using DREADDs (Designer Receptors Exclusively Activated by Designer Drugs) to control GPCR signaling specifically in neuronal cilia (Guo et al., 2017). DREADDs are mutant GPCRs (M3-muscarinic receptors) that have been molecularly evolved to be activated by the small molecule clozapine N-oxide (CNO). Our approach entails cilia-specific expression of a DREADD, $hM3D_q$, that couples to G_q and can induce Ca^{2+} activation when activated by CNO (Armbruster et al., 2007; Dong et al., 2010). Cilia-targeting-sequence [CLVCCWFKKSKTRKIKP] (Follit et al., 2010) was use the drive the ciliary localization of $hM3D_q$ (Cilia-$hM3D_q$). We have previously shown that Cilia-$hM3D_q$ triggers cilia-specific GPCR activation and related Ca^{2+} signaling (Guo et al., 2017). The expression of Cilia-$hM3D_q$ did not significantly change the length of primary cilia (Cilia-GFP: 2.72±0.10μm, Cilia-$hM3D_q$: 2.64±0.11μm, Student's *t*-test, p=0.56, n=14 neurons). Cilia-$hM3D_q$ and Ca^{2+} sensor RFP-GECO1.0 were co-expressed in DCN neurons. Upon 10μM CNO treatment, filopodial protrusions, correlated with Ca^{2+} elevation ($t_{1/2}$=8.34±3.13s, n=16 cells), start to emerge at the distal end of axons (Fig.5B–D). In contrast, control DMSO treatment did not change axonal growth cone dynamics or Ca^{2+} level (Fig.5B–D). Further, ACIII (Adenylate Cyclase III), a member of type III adenylate cyclase family that can potently induce cyclic AMP (cAMP), downstream of GPCR signaling activation, is selectively expressed in neuronal primary cilia. Optogenetic activation of a blue light-sensitive, cilia-targeted type III adenylyl cyclase ([Cilia-bPAC]; (Jansen et al., 2015; Stierl et al., 2011) led to cAMP induction and rapid filopodial protrusions (Fig.5E–F) similar to Cilia-$hM3D_q$ activation (Fig.5F–G). The expression of Cilia-bPAC did not significantly change the length of primary cilia (Cilia-GFP: 2.62±0.13μm, Cilia-bPAC: 2.96±0.12μm, Student's *t*-test, p=0.51, $n=12_{[Cilia\text{-}GFP]}$, $16_{[Cilia\text{-}bPAC]}$ neurons). In contrast, inhibition of ciliary ACIII activity with a modified, constitutively active, cilia-specific G_i-protein-coupled receptor, GPR88* (Siljee et al., 2018) in Arl13b-deficient neurons leads to opposite effects on filopodia/lamellipodial balance. GPR88* rescued the growth cone and filopodia phenotypes of the Arl13b-deficient neurons, reducing filopodial protrusions and increasing lamellipodial area (Fig. 5H–I). These results suggest that the activity of ciliary GPCRs can regulate axonal growth cone morphology and dynamics.

To address how the PI3K/AKT signaling, emanating from primary cilia, exerts its impact on axons, we generated optogenetic tools to gain precise, spatio-temporal control of ciliary-PI3K/AKT signaling in neurons and evaluated if selectively activating this signaling pathway in cilia can change axonal behavior (Fig.6A). The blue light activated, CIBN/CRY2 dimerization opto-system was used to selectively recruit PI3-kinase, phosphatidylinositol 5-phosphatase modules (5-Ptase module of Inpp5e), and AKT to cilia-membrane (Gradinaru et al., 2010; Idevall-Hagren et al., 2012; Katsura et al., 2015). This optogenetic system is based on blue-light (488nm)-induced dimerization between plant proteins, cryptochrome 2 (CRY2)

and the transcription factor CIBN (Idevall-Hagren et al., 2012). CIBN is expressed selectively in cilia using an established ciliary targeting sequence and is anchored to the ciliary plasma membrane through myristoylation (Su et al., 2013). CRY2 is fused to various second messenger modules. Blue light-induced dimerization between CRY2 and the ciliary membrane anchored CIBN (Cilia-CIBN) leads to the recruitment of these modules to cilia. The expression of Cilia-CIBN did not significantly change the length of primary cilia (Cilia-GFP: 2.93±0.22μm, Cilia-CIBN: 2.89±0.13μm, Student's *t*-test, p =0.82, n=$14_{[Cilia-GFP]}$, $15_{[Cilia-CIBN]}$ neurons).

We first examined if activating ciliary-PI3 kinase and generating PIP3 at the ciliary membrane will modulate axonal behavior. To do this, we generated cilia targeted CIBN (Cilia-CIBN-GFP), and co-expressed it with CRY2-iSH2, in which the inter-SH2 (iSH2) region of the p85α regulatory subunit of class I PI3-kinases is fused with CRY2, in DCN neurons (Idevall-Hagren et al., 2012). iSH2 constitutively binds to the endogenous catalytic p100α-subunit of PI3-kinase and with blue light stimulation the subunits are recruited along with iSH2 domain to the ciliary membrane (Fig.6A). In dark condition, CRY2-iSH2 is mostly enriched at the cytosol (Fig.6B). However, upon a train of 200ms blue laser (488nm) illumination solely focused on primary cilium, CRY2-iSH2 is rapidly recruited into the Cilia-CIBN-GFP expressing cilium ($t_{1/2}$=9±2.5s, n=16 cells) (Fig.6B). Co-expression the PIP3 reporter mCh-PH_{GRPI} with CRY2-iSH2 in these experiments allows simultaneous photo-activation and monitoring of PIP3 production. An increase of PIP3 within cilia was observed ($t_{1/2}$=93±14s, n=16 cells) following ciliary photo-activation (Fig.6C), confirming that ciliary recruitment of PI3 kinase is able to produce PIP3 in the ciliary membrane. We then analyzed the effect of ciliary PI3 kinase activation and PIP3 generation on axonal growth cones. The axonal growth cone dynamics were monitored before and after ciliary PI3 kinase activation in control DCN neurons. Before photo-activation, growth cones display characteristic lamellipodial webbing and short filopodial extensions (Fig.6D). Following blue light activation, growth cones changed their morphology and dynamics (24/29 cells), retracting lamellipodia while extending numerous aberrantly longer filopodial like protrusions, within 30 seconds of blue light illumination (Fig.6D–E). In contrast to the short-lived filopodial protrusions before photo-activation with a half-life time $t_{1/2}$=24 ±1.4s (n=24 cells), the filopodial protrusions formed after photo-activation are highly stable over the imaging duration (20 minutes). We confirmed that these axonal changes are not due to photo-toxicity induced by the photo-activation, since no changes in PIP3 level or growth cone dynamics were detected upon blue light illumination in neurons expressing only Cilia-GFP/CRY2-iSH2 and no Cilia-CIBN (SFig.7A–B). Further, ciliary photo-activation with non-blue light, or blue light illumination at comparably sized, non-ciliary regions in the neuronal soma did not change growth cone dynamics in neurons expressing Cilia-CIBN/CRY2-iSH2 or CIBN/CRY2-iSH2, respectively (SFig.7C–F). These results suggest that activation of ciliary PI3 kinase and the resultant production of ciliary PIP3 can rapidly induce changes in neuronal growth cone morphology and dynamics.

PI3-kinase activation and PIP3 production triggers AKT activation. To test if ciliary activation of AKT can induce similar changes in axonal dynamics, the kinase domain of AKT fused with CRY2 (mCh-CRY2-AKT; Katsura et al., 2015) was co-expressed with Cilia-CIBN-GFP in DCN neurons to enable blue light-induced AKT recruitment and

activation at the ciliary membrane (Fig.6F). Similar to PI3-kinase activation, mCh-CRY2-AKT showed rapid recruitment within the cilia upon ciliary blue light illumination ($t_{1/2}$=31±5.4s, n=16 cells) (Fig.6G), followed by axonal growth cone changes, including reduced growth cone area and extension of filopodial protrusions (Fig.6H–I).

In contrast to the enhancement of ciliary PIP3 production in the above experiments, we also tested the effect of ciliary recruitment of $5ptase_{INPP5E}$ to reduce ciliary PIP3 production (Fig.6J). mCh-CRY2–$5ptase_{INPP5E}$, containing the 5-Ptase catalytic module of Inpp5e necessary to hydrolyze PIP3 and PIP2, fused with CRY2, was co-expressed with Cilia-CIBN-GFP (Fig.6K). Ciliary blue light activation of these neurons induced a reduction of ciliary PIP3 (Fig.6L) ($t_{1/2}$=21±3.4s, n=16 cells), which is followed by retraction of filopodia and expansion of lamellipodia webbing (n=24 cells) (Fig. 6M, N). Ciliary activation of iSH2, AKT, or Inpp5e did not significantly change cilia length (Cilia length: $iSH2_{[before]}$=2.81±0.1μm, $iSH2_{[after]}$=2.78±0.1μm; $AKT_{[before]}$=2.93±0.2μm, $AKT_{[after]}$ =2.85±0.2μm; $Inpp5e_{[before]}$=2.87±0.3μm, $Inpp5e_{[after]}$=2.88±0.1μm; Student's *t*-test, p>0.05, n=16 cells/group). Together, these optogenetic manipulations of the ciliary-PI3K signaling reveal that this pathway has the capacity to rapidly and bi-directionally modulate axonal growth cone dynamics.

What are the signaling mechanisms that enable locally activated, ciliary-PI3K signaling to spread to axons? Recent studies show that AKT activation is sustained by a positive feedback loop mediated by PI3K activation and actin polymerization (Katsura et al., 2015). Feedback networks involving kinase-dependent cascades (e.g. PI3K and MAPK signaling) are known to self-perpetuate and rapidly spread local signaling over long distances along the plasma membrane to reach distant cellular targets (Fivaz et al., 2008; Katsura et al., 2015; Kholodenko, 2006; Sawano et al., 2002; Welf et al., 2012). To monitor the axonal changes in PIP3, post ciliary-PI3 kinase activation, axonal PIP3 reporters (RFP-PH_{AKT} or mCh-PH_{GRPI}) were imaged before and after ciliary activation of PI3-kinase. Both RFP-PH_{AKT} and mCh-PH_{GRPI} showed a gradual increase in the growth cones post activation, indicating lateral propagation of PI3K signaling (Fig.6O–P). Further, we noticed the ciliary activation of AKT is followed by a gradual increase of PIP3 in primary cilia and growth cones (Fig. 6Q–R). These data demonstrate that activated PI3K-AKT signaling in cilia can spread signal to axonal growth cones. Consistent with a role for positive feedback loops mediated by PI3K activation and actin polymerization in the propagation of such signaling, inhibition of actin polymerization with low dosage of Latrunculin B known to block AKT-PI3K feedback loop or inhibition of PI3-kinase activity with LY294002 abolished the increase of PIP3 at the growth cone and growth cone morphological changes induced by ciliary PI3K/AKT activation (SFig.7G–H).

Ciliary signaling regulated transcriptional landscape during axonal development

In addition to inducing rapid, local changes on axonal behavior, ciliary signaling may also impact transcriptional programs necessary for axonal development (Green and Mykytyn, 2014; McIntyre et al., 2012; Mukhopadhyay and Rohatgi, 2014; Wang et al., 2015). To gain further insights into the cilia signaling regulated transcriptional landscape during neuronal growth and connectivity, we performed RNAseq analysis of cortices dissected from E12.5

Arl13b$^{-/-}$ and littermate control embryos. This analysis identified 135 differentially expressed genes, 130 upregulated and 5 downregulated, in *Arl13b*$^{-/-}$ (SFig.8A). Gene Ontology (GO) analysis suggest that Arl13b deficiency leads to changes in the transcriptional landscape that converge onto biological processes including neural development/differentiation, cell adhesion, cytoskeleton organization, signal transduction, and metabolism (SFig.8B). Moreover, in support of our observation that PI3K/AKT signaling is a central driver of cilia signaling mediated changes in axonal development, IPA (Ingenuity pathway analysis) gene-gene interaction network analyses suggest that AKT is at the hub, inter-linking differentially expressed genes in Arl13b mutants (SFig.8C). This analysis of global transcriptional changes following *Arl13b* deletion further suggests a role for aberrantly activated PI3K/AKT and related signaling in the manifestation of axonal developmental changes in cilia mutants.

Discussion

Axonal tract defects are a common feature in many human ciliopathies, with JSRD exhibiting the most consistent and distinct axonal malformations such as MTS and abnormal CST organization. Here, using two, projection neuron-specific, JSRD mouse models, and cilia-specific, optogenetic and chemogenetic signaling approaches, we demonstrate that primary cilia driven signaling regulates proper growth cone dynamics and axonal development. Collectively, these results indicate that ciliary receptor activation and the resultant changes in convergent signaling cascades (e.g. PI3K, AKT, AC3) can effectively modulate of axonal behavior. These studies reveal a new cellular mechanism vital for the formation of neuronal connectivity in the mammalian brain and provide new insights into JSRD pathology.

Axonal defects related to JSRD

During the formation of the connectome in the brain, axons are guided by tropic and trophic gradients of chemoattractant or chemorepellent cues toward their target. Axons travel in large tracts or fascicles and follow stereotyped pathways to reach synaptic targets. Group extension of axons towards appropriate targets is necessary for neuronal wiring in the brain (Fame et al., 2011). Our observations show that while the axonogenesis or extension of axons are not affected in cilia mutants, the branching, fasciculation, crossing of axons and thus their accurate final projections are disrupted in cilia mutants.

Both a motile growth cone at the tip of the extending axon that properly responds to guidance cues and axon branching that enables axon sorting and fasciculation are crucial to ensure the fidelity of axonal tract development (Cioni et al., 2018; Nishikimi et al., 2013; Raper and Mason, 2010; Wang and Marquardt, 2013; Yu and Bargmann, 2001). Growth cone motility relies on the interplay between filopodia that sense environmental cues for pathfinding, and lamellipodia that support persistent axonal outgrowth (Mattila and Lappalainen, 2008; Mejillano et al., 2004; Vitriol and Zheng, 2012). Filopodia are necessary to initiate axon branches (Dent, 2004; Winkle et al., 2016). Branching along the axonal shafts enable projecting axons to connect with additional targets en route. Once reaching their appropriate final target, axons establish connections by extending terminal axon arbors

(Gibson and Ma, 2011; Kalil and Dent, 2014). We found that cilia mutant neurons show altered filopodia vs. lamellipodia balance and disrupted branching. Arl13b or Inpp5e-deficient neurons grow a long primary axon with significantly reduced lateral axonal branches and terminal arbors at targets, thus failing to sufficiently innervate their targets to form appropriate neuronal connections. These observations suggest that disruption of primary cilia mediated modulation of axonal growth cone and branching dynamics contributes to the axon-axon interaction and axonal path finding defects in cilia mutants. However, the nature of ciliary modulation of axonal response to guidance cues such as Netrin, Slit, Semaphorin, Ephrin, and Wnt during axonal pathfinding remains to be fully elucidated.

Patients with every ARL13B and INPP5E mutation suffer from intellectual disabilities and psychomotor delay. ARL13B^{G75R} mutant patients also suffer from epilepsy. While these neurological phenotypes clearly suggest circuit malfunction, apart from major axonal pathway defects detectable in MRI, other deficits such as neuronal dendritic disruptions are yet to be defined in genotyped JSRD patient brain tissue. Future studies focused on examining how these disease-causing mutations affect the interactions between ARL1B and INPP5E, as well as the interactome of ARL13B would be essential to further dissect the Arl13b-Inpp5e driven signaling mechanisms underlying JSRD.

Primary cilium as a signaling node during axonal development

Primary cilium, with a volume ~ 1/1000 of the soma, possesses diverse signaling machineries, including RTKs (e.g. IGFR, EGFR, PDGFR-α, Trk receptors p75^{NTR} and TrkB) and GPCRs (e.g. Smo, Frizzled receptor FZD3, Sstr3, 5HT6, NPY2R, NPY5R, D2, MchR1, GPR161), their downstream effectors (e.g. PI3 kinase, Inpp5b, Inpp5e, Ocrl, AKT, CaMKIIβ, AC3, 5 and 6), and second messengers (e.g. PIP3, PIP2, Ca^{2+} and cAMP), thus providing a unique environment where signaling components are highly concentrated in a small cellular domain to facilitate efficient signaling activation and crosstalk (Arellano et al., 2012; Armato et al., 2011; Choi et al., 2011; Christensen et al., 2012; Conduit et al., 2012; DeCaen et al., 2013; Delling et al., 2013; Franco et al., 2014; Green and Mykytyn, 2014; Guo et al., 2015; Hilgendorf et al., 2016; Jacoby et al., 2009; Mukhopadhyay and Rohatgi, 2014; Nichols et al., 2013; Omori et al., 2015; Phua et al., 2015; Puram et al., 2011; Schou et al., 2015; Zhu et al., 2009). However, due to the lack of methods to exert precise control of cilia-specific signaling events, the exact cellular and physiological impact of the signaling emanating from primary cilia on the developing neurons and neural circuit formation remained poorly understood. To overcome this limitation, we employed a combination of mouse genetics, chemogenetic and optogenetic approaches to enable the interrogation of ciliary signaling in the developing neurons. Collectively, our observations suggest that altered ciliary PI3K/AKT signaling homeostasis underlies the aberrant axonal growth cone dynamics in cilia mutant neurons and that signals emanating from cilia have the capacity to remotely regulate axonal growth cone behavior changes over long distance, via a yet-to-be defined modes of propagation.

Propagation of ciliary signaling in neurons

Deficiency of Inpp5e, the main inositol polyphosphate-5-phosphatase within cilia, disrupts the ciliary membrane phosphoinositide (PIP/PIP2/PIP3) composition and results in dysregulation of Shh and PI3K/AKT signaling (Chavez et al., 2015; Conduit et al., 2012; Dyson et al., 2017; Eramo and Mitchell, 2016; Garcia-Gonzalo et al., 2015). Our observations show that Inpp5e deficiency caused by *Arl13b* or *Inpp5e* deletion leads to globally elevated PIP3 level and PI3K/AKT activity in developing neurons, supporting the notion that dysregulated ciliary signaling can propagate throughout the whole neuronal cell body to manifest pathogenic changes in normal state.

Once activated, PI3K/AKT signaling employs downstream kinase cascades and second messengers (e.g. Ca^{2+}, cAMP, IP3, PIP3) to amplify and propagate signals for cell-wide, long-distance signaling (Civelli, 2012; Fruman et al., 2017; Gavi et al., 2006; Lemmon and Schlessinger, 2010). We show that ciliary GPCR signaling induces axonal Ca^{2+} wave down to the growth cone. Previous studies suggest that Shh-Smo signaling, possibly via primary cilia, act to down regulate cAMP levels and protein kinase A activity in commissural neurons to allow Sema3 mediated repulsion of axons at midline crossing (Parra and Zou, 2010). The exact mechanisms that enable ciliary signaling to trigger axonal Ca^{2+} wave and its integration with axonal PI3K/AKT signaling waves are yet to be fully elucidated. Nevertheless, our observations indicate that ciliary signaling can engage multiple convergent pathways to enable signal propagation across the neuronal cell body.

Primary cilia signaling is likely to influence neuronal behavior via both rapid local signaling cascade changes as well as by triggering changes in transcriptional programs underlying neuronal growth and connectivity. Considering the time window it takes for long projecting axons to grow, navigate, and connect with their distant targets (i.e., several days), primary cilia signaling driven local changes may facilitate rapid fine tuning of axonal behavior, whereas transcriptional program changes may facilitate permissive conditions for axon growth, navigation, and target recognition. PI3/AKT signaling, in addition to locally changing axonal behavior, is also known to directly regulate transcriptional networks important for axonal development (Chen et al., 2014; Graef et al., 2003; Kwon et al., 2006; Nguyen and Di Giovanni, 2008; Manning and Toker, 2017; Sánchez-Alegría et al., 2018). It is thus conceivable that PI3K/AKT signaling serves as a converging node to integrate ciliary receptor signaling necessary for both rapid axonal tract growth modulation and long-term neuronal developmental program regulation.

This study points to the tantalizing possibility that neuronal primary cilia may customize a “ciliary signaling signature” that elicits cilia-specific impact on neuronal events such as calcium waves, cytoskeletal rearrangements, adhesion, and transcriptional regulation necessary for proper axonal tract development and wiring. In spite of not being required for extension of axons, cilia appear to exert a crucial modulatory role in appropriate axonal wiring. Cilia signaling, from locales where the neuronal soma are, may enable fine tuning of projection neuron axonal behavior, long distances away, necessary to establish the final axonal connectivity. Cilia may thus serve as modulators that enable coordination of signaling between neuronal origin and target (e.g., DCN and thalamus or cortical projection neuron and spinal cord) necessary to establish precise patterns of connectivity. Consistent with this,

our observations show that neuronal cilia regulate axonal growth cones, at the tip of axonal projections, whose functions are necessary for precise wiring of the neural circuitry. Future efforts to decipher the communication networks between neuronal cilia and their cellular environment or between axons and cilia, in the context of brain development, will facilitate a holistic view of how primary cilia receive and convey environmental signals to modulate brain formation and organization. Nevertheless, our studies delineate the significance of cilia driven signaling in axonal tract development and connectivity in the developing brain, thus defining a hitherto undefined cell biological mechanism fundamental for neuronal circuit formation in the brain and whose dysregulation may underlie axonal tract defects in Joubert Syndrome Related Disorders.

STAR Methods

Contact for Reagent and Resource Sharing

Further information and requests for resources and reagents should be directed to, and will be fulfilled by the lead contact, E. S. Anton (anton@med.unc.edu).

Experimental Model and Subject Details

Mice—This study is based on data from mice at various developmental stages (embryonic days 16, 18, postnatal days 1, 7, 30, and 60) and includes both males and females. Mice were cared for according to animal protocols approved by the University of North Carolina. Arl13b or Inpp5e was conditionally inactivated in cortical projection neurons and deep cerebellar nuclei by crossing *Arl13b*$^{Lox/Lox}$ mice (Arl13b^{tm1Tc}, MGI: 4948239) (Su et al., 2012) or *Inpp5e*$^{Lox/Lox}$ (Inpp5e^{tm1Ssch}, MGI:4360185) (Jacoby et al., 2009) with Nex-Cre mice (Goebbels et al., 2006). Further, transgenic mice carrying the Tau-Lox-STOP-Lox-GFP cassette (Hippenmeyer et al., 2005) or Ai9 reporter (Madisen et al., 2010) were bred into the *Arl13b*$^{Lox/+}$*; Nex-Cre* and *Inpp5e*$^{Lox/+}$*; Nex-Cre* lines. Cre recombination of the *Tau-Lox-STOP-Lox-mGFP* or Ai9 transgene leads to GFP or mRFP expression, respectively, in the processes of all Cre-positive neurons. *Arl13b*$^{Lox/+}$*; Nex-Cre* or *Inpp5e*$^{Lox/+}$*; Nex-Cre* littermates served as controls. Arl13b null mice (*Arl13b*$^{-/-}$ or *Arl13b*^{hnn}; MGI:3578151), Ift88 null mice (Ift88$^{tm1.1Bky}$, MGI: 3710186), Inpp5e^{M2} mice (MGI: 5296378) were generated as described in Caspary et al., 2007, Haycraft et al., 2007, and Su et al., 2012, respectively. All lines were genotyped as previously described (Caspary et al., 2007; Su et al., 2012; Higginbotham et al., 2013). Location of different anatomical regions of the mouse brain were annotated using the mouse brain atlas (Paxinos and Franklin, 2001).

DNA constructs—CIBN-GFP, CRY2-iSH2, mCh-CRY2-iSH2, mCherry-CRY2–5Ptase$_{INPP5E}$, CRY2–5Ptase$_{INPP5E,}$ RFP-PH$_{AKT}$, and mCh-PH$_{GRPI}$ (Idevall-Hagren et al., 2012) are gifts from Dr. Pietro De Camilli, Yale University. The cilia targeted CIBN-GFP was generated by replacing R-GECO1.0 in IA-R-GECO1.0 with CIBN-GFP. IA-R-GECO1.0 (Su et al., 2013) is a gift from Dr. Takanari Inoue, John Hopkins University. CRY2-venus-AKT1 (Katsura et al., 2015) is a gift from Dr. Takeaki Ozawa (the University of Tokyo). mCh-CRY2-AKT1 was generated by replacing 5Ptase$_{INPP5E}$ with AKT1 in mCherry-CRY2–5Ptase$_{INPP5E}$. The cilia-targeted bPAC (cilia-bPAC) (Jansen et al., 2015) is a gift from Dr. Dagmar Wachten (Center of Advanced European Studies and Research,

Bonn, Germany). pAAV-DIO-FLAG-GPR88* (Siljee et al, 2018) is a generous gift from Dr. Christian Vaisse (The University of California, San Francisco). Pcdh17-GFP (Hayashi et al., 2014) is a generous gift from Dr. Masatoshi Takeichi (RIKEN Center for Developmental Biology). The Cre-inducible adeno-associated virus (AAV) vectors expressing ARL13B variants and mCherry were generated as described previously (Guo et al., 2017). The AAV5-Synapsin-tdTomato virus (Klapoetke et al., 2014) was obtained from UNC viral vector core.

CLARITY imaging—CLARITY experiments were performed based on protocols available at: http://wiki.claritytechniques.org/index.php/Solutions. Briefly, *Arl13b*$^{Lox/lox}$*-NexCre-Ai9* and control pups (P1) were perfused with ice cold 4% PFA. Brains with spinal cords attached were dissected and post fixed in 4% PFA overnight at 4 °C, followed by incubation in 30ml hydrogel solution for 2 days at 4 °C. Following polymerization of the hydrogel monomers, samples were incubated with clearing solution for 2 weeks at 37 °C. Cleared samples were washed with PBST (0.1% TritonX in 1X PBS) buffer for 2 days and stored in PBST at 4 °C. For CLARITY imaging, samples were incubated with 85% glycerol for 1h, placed in a glass bottom FluoroDIsh chambers (World Precision Instruments, Inc.) filled with 85% glycerol and imaged using a Zeiss780 confocal microscope equipped with 10x objectives.

Microfluidic chamber assay—Microfluidic chambers (Higginbotham et al., 2012) were attached to laminin coated glass coverslips. 5μl containing 200K cells from DCN of P3 *Arl13b*$^{Lox/+}$*; NexCre* or *Arl13b*$^{Lox/Lox}$*; NexCre* brains electroporated with BFP (Addgene #127348) plasmids were seeded onto one side of the microfluidic chamber. 24 hours later, the same number of cells from P3 *Arl13b*$^{Lox/+}$*; NexCre; Ai9* or *Arl13b*$^{Lox/Lox}$*; NexCre; Ai9* brains electroporated with Pcdh17-EGFP were seeded onto the opposite chamber. Cells were maintained at 37°C/5% CO2 and 10μl of new media (DMEM/N2/B27) was added every 24 hours. After 48 hours, cells were fixed in 4% paraformaldehyde and analyzed for the expression pattern of Pcdh17-EGFP at BFP^{+}/tdTom^{+} axon-axon contacts.

***In utero* electroporation—**Lateral ventricles of *Arl13b*$^{Lox/+}$ and *Arl13b*$^{Lox/Lox}$, or *Inpp5e*$^{Lox/+}$ and *Inpp5e*$^{Lox/Lox}$ (E15.5) embryos were electroporated as described previously (Guo et al., 2015; Higginbotham et al., 2012). Briefly, 1μl of CAG-Cre (Addgene #13775) and CAG-GFP (Addgene #16664) plasmid DNA (2 μg/μl) was injected into the lateral ventricles of E15.5 brains and electroporated using 5 pulses at 30 V for 50 ms at 950 ms intervals through the uterine wall using a BTX ElectroSquarePorator (ECM 830). Embryos were then allowed to develop *in vivo* and analyzed at P1 or P21. Plasmids used for *in utero* electroporation were prepared using the EndoFree Plasmid kit (Qiagen).

Primary Neuronal Culture and transfection—Deep cerebellar nuclei (P2) or dorsal cortices (E15) were dissected in Hank's buffered salt solution (HBSS), dissociated in HBSS containing papain (Worthington) and DNase I (100 mg/ml, Sigma) for 10 min at 37C, washed in HBSS three times and manually triturated in Neural basal medium supplemented with DNase I. Neurons from E11.5 or 12.5 cortices were similarly processed. Neurons were transfected using Amaxa™Nuleofector™ II kit (Lonza) or Invitrogen Lipofectamine 2000 reagent according to the manufacturer's protocol. 1.0×10^4 cells were plated per 35 mm

glass bottom dish (MatTek) coated with poly-L-lysine /Laminin (Sigma) and cultured for 1–4 days in Neurobasal-A /5% B27/1% GlutaMax/1% P/S media.

Chemogenetic manipulation of ciliary signaling and axonal imaging—Cultured DCN neurons were transfected with R-GECO1.0 and Cilia-hM3D$_q$ and imaged at an acquisition rate of 0.5 Hz using a Zeiss 780 live cell confocal microscope. The effects of CNO or DMSO on axonal Ca^{2+} and growth cone behavior were assessed in neurons expressing Ciliary hM3D$_q$ by recording upto 20min before and 20min after addition. GECO1.0 fluorescence intensity values were normalized against background and the average baseline values were measured prior to CNO or DMSO addition. Image analysis was performed using Zeiss LSM Image Browser or ImageJ software.

Optogenetic manipulation of ciliary-PI3K/AKT, ciliary-Adenylyl cyclase signaling and axonal imaging—For ciliary-PI3K activation, cultured DCN neurons were transfected with Cilia-GFP-CIBN, mCh-CRY2-iSH2, or CRY2-iSH2. For ciliary-AKT activation, DCN neurons were transfected with Cilia-GFP-CIBN, mCh-CRY2-AKT1, or CRY2-venus-AKT1. For ciliary-Inpp5e$_{5ptase}$ activation, DCN neurons were transfected with Cilia-GFP-CIBN and mCh-CRY2–5ptase-Inpp5e. RFP-PH$_{AKT}$ or mCh-PH$_{GRPI}$ were used as PIP3 sensors. For ciliary-bPAC activation, DCN neurons were transfected with mCh-Sstr3-bPAC and pcDNA3.1-BFP. A train of 200ms blue laser light (488nm) focused on primary cilia for upto 3 minutes was used to induce dimerization between CRY2 and CIBN within primary cilia (Idevall-Hagren et al., 2012). Growth cone morphology and dynamics were imaged with 561nm laser (mCh or mRFP) at an acquisition rate of 0.5 Hz upto 20min before and 20min after photo-activation using a Zeiss 780 live cell confocal microscope. The imaging positions and parameters for primary ciliary light activation and growth cone imaging was setup using the multi-position, time series, and photo bleaching applications in ZEN software.

Immunohistochemistry—Cerebral cortical sections and neurons were immunolabeled as previously described (Guo et al., 2017; Schmid et al., 2003; Weimer et al., 2008; Yokota et al., 2007) with the following primary antibodies: anti-GFP (chicken, 1:1000; Abcam, ab13970), anti-RFP (rabbit, 1:500; Rockland, cat. nr. 600–401-379), anti-ACIII (rabbit polyclonal, 1:100; Santa Cruz, sc-56855), anti-Tau (mouse 1:1000, Millipore, MAB3420), anti-Map2 (chicken polyclonal, 1:1000, Abcam, ab5392), Immunoreactivity was detected by incubation with appropriate AlexaFluor 488 or Cy3-conjugated secondary antibodies (Invitrogen and Jackson ImmunoResearch). AlexaFluor 488, 647 or Cy3-conjugated (Invitrogen and Jackson ImmunoResearch) secondary antibodies were used. Nuclei were counterstained with DAPI (Sigma).

Tissue Culture and transfection—Mouse embryonic fibroblast (MEF) cells were derived from wild type and *Arl13b*$^{-/-}$ E12.5 embryos as previously described (Higginbotham et al., 2012). MEF cells and IMCD3 (authenticated by American Type Culture Collection [ATCC]) were grown in DMEM/ F12 media supplemented with 10% fetal bovine serum (FBS) and 1% penicillin/streptomycin (P/S) at 37°C/5% CO_2. Cells were allowed to reach 80% confluency and ciliogenesis was induced by serum starvation for 24

hours. Cells were then transfected using Invitrogen Lipofectamine 2000 reagent according to manufacture's instructions.

Immunoblotting—Cortices of Arl13b null and control embryos (E12) or cultured cells were harvested in 200 μl cell lysis buffer (Cell signaling, #9803) with protease and phosphatase inhibitor cocktail (Thermo Scientific). The lysates were briefly sonicated and centrifuged at 14,000 rpm for 20 min at 4°C. Protein concentrations were determined using the protein assay reagent (Bio-Rad). Samples were mixed with 3X SDS sample buffer and boiled for 5 min. Samples were then resolved in SDS-polyacrylamide gels, transferred to nitrocellulose, and incubated with following primary antibodies: rabbit anti-pAKT [Thr308] (1:1000, Cell signaling, #9275), rabbit anti-pGSK3β (1:1000, Cell signaling, #9331), rabbit anti-pS6 (1:1000, Cell signaling, #4858), rabbit anti-AKT (1:1000, Cell signaling, #9272), mouse anti-β-actin (1:1000, Abcam, ab8226). Immunoblots were developed using horseradish peroxidase-conjugated goat anti-mouse or goat anti-rabbit IgG, followed by detection with enhanced chemiluminescence.

RNA-seq—RNA was isolated *from E12.5 control and Arl13b*$^{-/-}$ *cortices* with the RNeasy plus mini kit (Cat. #74134, Qiagen). RNA yield and quality was determined with a Nanodrop 1000 Spectrophotometer (Thermo Scientific). RNA quality was further assessed by an Agilent Bioanalyzer 2100 to obtain a RNA integrity number (RIN). RIN values exceeding 8 were used for sequencing. RNA samples were used to generate and barcode cDNA libraries using the Nugen ovation RNAseq Plus Kit at the UNC High Throughput Sequencing Facility. Pool of 6 samples were sequenced in a single lane in a HiSeq 4000 sequencer (Illumina) using 50 bp paired-end reads.

Image analysis—All images were analyzed using ImageJ (NIH) and Zeiss Zen. Kymographs and fluorescence intensity of Ca^{2+} sensors RFP-GECO1.0 or IA-GFP-GECO1.0, and PIP3 sensors RFP-PH_{AKT} or mCh-PH_{GRPI} were quantified using ImageJ (Guo et al., 2017). ROIs located in cilia, soma, or growth cones of neurons were selected and the mean value of fluorescence intensity of ROIs (after background subtraction) over time was plot profiled. For the turning angle measurement of SCP, lines were drawn along the SCP tract pre and post turning and the turning angle was quantified using the angle tool in Image J.

RNA-seq data analysis—Reads were filtered for quality using the FASTX toolkit's fastq_quality_filter (http://hannonlab.cshl.edu/fastx_toolkit/index.html) with 90% of the bases having a minimal quality score of 20. Sequencing adaptors were trimmed using cutadapt. Reads were aligned to the mm9 reference genome using STAR. Transcript abundance was estimated using Salmon (Patro et al., 2017). DESeq2 was used to normalize read depth and calculate differential gene expression. Genes with a Benjamini-Hochberg (B&H) FDR adjusted p-value < 0.05, fold change > 2 or <−2 were considered significant. GO term annotation of gene lists was performed using ToppGene. GO terms with a B&H FDR adjusted p-value < 0.05 were considered significant. Lists of significant GO terms were clustered using REVIGO. Ingenuity Pathway Analysis (IPA) [https://

www.qiagenbioinformatics.com/products/ingenuity-pathway-analysis] was used for pathway analysis, novel network identification, and upstream regulator analysis.

Quantification and Statistical Analysis

General statistical analysis—GraphPad or Excel was used for data analysis. Two-tailed Student's *t* test and ANOVA were performed using GraphPad. No *a priori* power analyses were performed, but sample sizes were similar to those described in previous related studies (Guo et al., 2015; Guo et al., 2017; Higginbotham et al., 2012, 2013). All experiments were independently repeated for at least 3 or more times. All data are expressed as means ± standard error of the mean (SEM). Statistical details, including p values, are indicated in text or figure legends.

Data and Code Availability

The published article includes all datasets generated or analyzed during this study. RNA-seq data were deposited in the GEO database (GSE120310).

Supplementary Material

Refer to Web version on PubMed Central for supplementary material.

Acknowledgements

This research was supported by NIH grant NS090029 to EA and TC, Natural Sciences and Engineering Research Council of Canada grant RGPIN-2019-04820 to JG, F31 NS101806 and T32GM008490 to SKS, and the confocal imaging core of NINDS grant 5P30NS045892. We thank A. Kolodkin and A. S. LaMantia for helpful comments.

References

Arellano JI, Guadiana SM, Breunig JJ, Rakic P, and Sarkisian MR (2012). Development and distribution of neuronal cilia in mouse neocortex. Journal of Comparative Neurology 520, 848–873. [PubMed: 22020803]

Armato U, Chakravarthy B, Chiarini A, Prà ID, and F Whitfield J (2011). A Paradigm-changing surprise from dentate gyrus granule cells—cilium-localized p75NTR may drive their progenitor cell proliferation. J Alzheimers Dis 01, 1–3.

Armbruster BN, Li X, Pausch MH, Herlitze S, and Roth BL (2007). Evolving the lock to fit the key to create a family of G protein-coupled receptors potently activated by an inert ligand. Proceedings of the National Academy of Sciences 104, 5163–5168.

Banker G (2018). The Development of Neuronal Polarity: A Retrospective View. The Journal of neuroscience : the official journal of the Society for Neuroscience 38, 1867–1873. [PubMed: 29467146]

Barral DC, Garg S, Casalou C, Watts GFM, Sandoval JL, Ramalho JS, Hsu VW, and Brenner MB (2012). Arl13b regulates endocytic recycling traffic. Proceedings of the National Academy of Sciences of the United States of America 109, 21354–21359. [PubMed: 23223633]

Bielas SL, Silhavy JL, Brancati F, Kisseleva MV, Al-Gazali L, Sztriha L, Bayoumi RA, Zaki MS, Abdel-Aleem A, Rosti RO, et al. (2009). Mutations in INPP5E, encoding inositol polyphosphate-5-phosphatase E, link phosphatidyl inositol signaling to the ciliopathies. Nature Genetics 41, 1032–1036. [PubMed: 19668216]

Brancati F, Dallapiccola B, and Valente E (2010). Joubert Syndrome and related disorders. Orphanet Journal of Rare Diseases 5, 20–10. [PubMed: 20615230]

Cantagrel V, Silhavy JL, Bielas SL, Swistun D, Marsh SE, Bertrand JY, Audollent S, Attie-Bitach T, Holden KR, Dobyns WB, et al. (2008). Mutations in the cilia gene ARL13B lead to the classical form of Joubert syndrome. Am J Hum Genet 83, 170–179. [PubMed: 18674751]

Caspary T, Larkins CE, and Anderson KV (2007). The Graded Response to Sonic Hedgehog Depends on Cilia Architecture. Developmental Cell 12, 767–778. [PubMed: 17488627]

Chavez M, Ena S, Van Sande J, de Kerchove d'Exaerde A, Schurmans S, and Schiffmann SN (2015). Modulation of Ciliary Phosphoinositide Content Regulates Trafficking and Sonic Hedgehog Signaling Output. Dev Cell 34, 338–350. [PubMed: 26190144]

Chedotal A, and Richards LJ (2010). Wiring the Brain: The Biology of Neuronal Guidance. Cold Spring Harbor Perspectives in Biology 2, a001917–a001917. [PubMed: 20463002]

Chen J, Alberts I, and Li X (2014). Dysregulation of the IGF-I/PI3K/AKT/mTOR signaling pathway in autism spectrum disorders. International journal of developmental neuroscience : the official journal of the International Society for Developmental Neuroscience 35, 35–41. [PubMed: 24662006]

Choi Y-H, Suzuki A, Hajarnis S, Ma Z, Chapin HC, Caplan MJ, Pontoglio M, Somlo S, and Igarashi P (2011). Polycystin-2 and phosphodiesterase 4C are components of a ciliary A-kinase anchoring protein complex that is disrupted in cystic kidney diseases. Proceedings of the National Academy of Sciences of the United States of America 108, 10679–10684. [PubMed: 21670265]

Christensen ST, Clement CA, Satir P, and Pedersen LB (2012). Primary cilia and coordination of receptor tyrosine kinase (RTK) signalling. The Journal of Pathology 226, 172–184. [PubMed: 21956154]

Cioni J-M, Wong HH-W, Bressan D, Kodama L, Harris WA, and Holt CE (2018). Axon-Axon Interactions Regulate Topographic Optic Tract Sorting via CYFIP2-Dependent WAVE Complex Function. Neuron 97, 1078–1093.e1076. [PubMed: 29518358]

Civelli O (2012). Orphan GPCRs and Neuromodulation. Neuron 76, 12–21. [PubMed: 23040803]

Conduit SE, Dyson JM, and Mitchell CA (2012). Inositol polyphosphate 5-phosphatases; new players in the regulation of cilia and ciliopathies. FEBS Letters 586, 2846–2857. [PubMed: 22828281]

DeCaen PG, Delling M, Vien TN, and Clapham DE (2013). Direct recording and molecular identification of the calcium channel of primary cilia. Nature 504, 315–318. [PubMed: 24336289]

Delling M, DeCaen PG, Doerner JF, Febvay S, and Clapham DE (2013). Primary cilia are specialized calcium signalling organelles. Nature 504, 311–314. [PubMed: 24336288]

Dent EW, Barnes AM, Tang F, and Kalil K (2004). Netrin-1 and semaphorin 3A promote or inhibit cortical axon branching, respectively, by reorganization of the cytoskeleton. J. Neurosci 24, 3002–3012. [PubMed: 15044539]

Dong S, Allen JA, Farrell M, and Roth BL (2010). A chemical-genetic approach for precise spatio-temporal control of cellular signaling. Molecular BioSystems 6, 1376–1375. [PubMed: 20532295]

Dyson JM, Conduit SE, Feeney SJ, Hakim S, DiTommaso T, Fulcher AJ, Sriratana A, Ramm G, Horan KA, Gurung R, et al. (2017). INPP5E regulates phosphoinositide-dependent cilia transition zone function. J Cell Biol 216, 247–263. [PubMed: 27998989]

Engle EC (2010). Human Genetic Disorders of Axon Guidance. Cold Spring Harbor Perspectives in Biology 2, a001784–a001784. [PubMed: 20300212]

Eramo MJ, and Mitchell CA (2016). Regulation of PtdIns(3,4,5)P3/Akt signalling by inositol polyphosphate 5-phosphatases. Biochemical Society Transactions 44, 240–252. [PubMed: 26862211]

Fame RM, MacDonald JL, and Macklis JD (2011). Development, specification, and diversity of callosal projection neurons. Trends in Neurosciences 34, 41–50. [PubMed: 21129791]

Fivaz M, Bandara S, Inoue T, and Meyer T (2008). Robust Neuronal Symmetry Breaking by Ras-Triggered Local Positive Feedback. Current Biology 18, 44–50. [PubMed: 18158244]

Follit JA, Li L, Vucica Y, and Pazour GJ (2010). The cytoplasmic tail of fibrocystin contains a ciliary targeting sequence. J Cell Biol. 188, 21–8. [PubMed: 20048263]

Franco I, Gulluni F, Campa CC, Costa C, Margaria JP, Ciraolo E, Martini M, Monteyne D, De Luca E, Germena G, et al. (2014). PI3K class II alpha controls spatially restricted endosomal PtdIns3P and Rab11 activation to promote primary cilium function. Dev Cell 28, 647–658. [PubMed: 24697898]

Fruman DA, Chiu H, Hopkins BD, Bagrodia S, Cantley LC, and Abraham RT (2017). The PI3K Pathway in Human Disease. Cell 170, 605–635. [PubMed: 28802037]

Garcia-Gonzalo FR, Phua SC, Roberson EC, Garcia G 3rd, Abedin M, Schurmans S, Inoue T, and Reiter JF (2015). Phosphoinositides Regulate Ciliary Protein Trafficking to Modulate Hedgehog Signaling. Dev Cell 34, 400–409. [PubMed: 26305592]

Gavi S, Shumay E, Wang H. y., and Malbon CC (2006). G-protein-coupled receptors and tyrosine kinases: crossroads in cell signaling and regulation. Trends in Endocrinology & Metabolism 17, 48–54.

Gibson DA, and Ma L (2011). Developmental regulation of axon branching in the vertebrate nervous system. Development 138, 183–195. [PubMed: 21177340]

Goebbels S, Bormuth I, Bode U, Hermanson O, Schwab MH, and Nave K-A (2006). Genetic targeting of principal neurons in neocortex and hippocampus of NEX-Cre mice. genesis 44, 611–621. [PubMed: 17146780]

Gradinaru V, Zhang F, Ramakrishnan C, Mattis J, Prakash R, Diester I, Goshen I, Thompson KR, and Deisseroth K (2010). Molecular and Cellular Approaches for Diversifying and Extending Optogenetics. Cell 141, 154–165. [PubMed: 20303157]

Graef IA, Wang F, Charron F, Chen L, Neilson J, Tessier-Lavigne M, and Crabtree GR (2003). Neurotrophins and netrins require calcineurin/NFAT signaling to stimulate outgrowth of embryonic axons. Cell 113, 657–70. [PubMed: 12787506]

Green JA, and Mykytyn K (2014). Neuronal primary cilia: an underappreciated signaling and sensory organelle in the brain. Neuropsychopharmacology : official publication of the American College of Neuropsychopharmacology 39, 244–245. [PubMed: 24317320]

Green WW, Uytingco CR, Ukhanov K, Kolb Z, Moretta J, McIntyre JC, and Martens JR (2018). Peripheral Gene Therapeutic Rescue of an Olfactory Ciliopathy Restores Sensory Input, Axonal Pathfinding, and Odor-Guided Behavior. J Neurosci. 38, 7462–7475. [PubMed: 30061191]

Guadiana SM, Semple-Rowland S, Daroszewski D, Madorsky I, Breunig JJ, Mykytyn K, and Sarkisian MR (2013). Arborization of Dendrites by Developing Neocortical Neurons Is Dependent on Primary Cilia and Type 3 Adenylyl Cyclase. Journal of Neuroscience 33, 2626–2638. [PubMed: 23392690]

Guemez-Gamboa A, Coufal NG, and Gleeson JG (2014). Primary Cilia in the Developing and Mature Brain. Neuron 82, 511–521. [PubMed: 24811376]

Guo J, Higginbotham H, Li J, Nichols J, Hirt J, Ghukasyan V, and Anton ES (2015). Developmental disruptions underlying brain abnormalities in ciliopathies. Nature communications 6, 1–13.

Guo J, Otis JM, Higginbotham H, Monckton C, Cheng J, Asokan A, Mykytyn K, Caspary T, Stuber GD, and Anton ES (2017). Primary Cilia Signaling Shapes the Development of Interneuronal Connectivity. DEVCEL 42, 286–300.e284.

Hakim S, Bertucci MC, Conduit SE, Vuong DL, and Mitchell CA (2012). Inositol polyphosphate phosphatases in human disease. Current topics in microbiology and immunology 362, 247–314. [PubMed: 23086422]

Hayashi S, Inoue Y, Kiyonari H, Abe T, Misaki K, Moriguchi H, Tanaka Y, and Takeichi M (2014). Protocadherin-17 Mediates Collective Axon Extension by Recruiting Actin Regulator Complexes to Interaxonal Contacts. DEVCEL 30, 673–687.

Haycraft CJ, Zhang Q, Song B, Jackson WS, Detloff PJ, Serra R, and Yoder BK (2007). Intraflagellar transport is essential for endochondral bone formation. Development 134, 307–316. [PubMed: 17166921]

Henle SJ, Wang G, Liang E, Wu M, Poo M.m., and Henley JR (2011). Asymmetric PI(3,4,5)P3 and Akt Signaling Mediates Chemotaxis of Axonal Growth Cones. Journal of Neuroscience 31, 7016–7027. [PubMed: 21562263]

Higginbotham H, Eom T-Y, Mariani LE, Bachleda A, Hirt J, Gukassyan V, Cusack CL, Lai C, Caspary T, and Anton ES (2012). Arl13b in primary cilia regulates the migration and placement of interneurons in the developing cerebral cortex. Developmental Cell 23, 925–938. [PubMed: 23153492]

Higginbotham H, Guo J, Yokota Y, Umberger NL, Su C-Y, Li J, Verma N, Hirt J, Ghukasyan V, Caspary T, et al. (2013). Arl13b-regulated cilia activities are essential for polarized radial glial scaffold formation. Nature neuroscience, 1–9. [PubMed: 23232605]

Hildebrandt F, Benzing T, and Katsanis N (2011). Ciliopathies. N Engl J Med 364, 1533–1543. [PubMed: 21506742]

Hilgendorf KI, Johnson CT, and Jackson PK (2016). The primary cilium as a cellular receiver: organizing ciliary GPCR signaling. Curr Opin Cell Biol 39, 84–92. [PubMed: 26926036]

Hippenmeyer S, Vrieseling E, Sigrist M, Portmann T, Laengle C, Ladle DR, and Arber S (2005). A Developmental Switch in the Response of DRG Neurons to ETS Transcription Factor Signaling. PLOS Biology 3, e159–113. [PubMed: 15836427]

Hoshina N, Tanimura A, Yamasaki M, Inoue T, Fukabori R, Kuroda T, Yokoyama K, Tezuka T, Sagara H, Hirano S, et al. (2013). Protocadherin 17 Regulates Presynaptic Assembly in Topographic Corticobasal Ganglia Circuits. Neuron 78, 839–854. [PubMed: 23684785]

Humbert MC, Weihbrecht K, Searby CC, Li Y, Pope RM, Sheffield VC, and Seo S (2012). ARL13B, PDE6D, and CEP164 form a functional network for INPP5E ciliary targeting. Proceedings of the National Academy of Sciences of the United States of America 109, 19691–19696. [PubMed: 23150559]

Idevall-Hagren O, Dickson EJ, Hille B, Toomre DK, and De Camilli P (2012). Optogenetic control of phosphoinositide metabolism. Proceedings of the National Academy of Sciences of the United States of America 109, E2316–2323. [PubMed: 22847441]

Iskender CT, Tarim E, and Alkan O (2012). Joubert syndrome and related disorders, prenatal diagnosis with ultrasound and magnetic resonance imaging. J Turk Ger Gynecol Assoc 13, 135–138. [PubMed: 24592023]

Jacoby M, Cox JJ, Gayral S, Hampshire DJ, Ayub M, Blockmans M, Pernot E, Kisseleva MV, Compere P, Schiffmann SN, et al. (2009). INPP5E mutations cause primary cilium signaling defects, ciliary instability and ciliopathies in human and mouse. Nat Genet 41, 1027–1031. [PubMed: 19668215]

Siljee JE, Bernard AA, Ersoy BA, Zhang S, Marley A, Von Zastrow M, Reiter JF, and Vaisse C (2018). Subcellular localization of MC4R with ADCY3 at neuronal primary cilia underlies a common pathway for genetic predisposition to obesity. Nature Genetics 50, 180–185. [PubMed: 29311635]

Jansen V, Alvarez L, Balbach M, Strunker T, Hegemann P, Kaupp UB, and Wachten D (2015). Controlling fertilization and cAMP signaling in sperm by optogenetics. Elife 4.

Juric-Sekhar G, Adkins J, Doherty D, and Hevner RF (2012). Joubert syndrome: brain and spinal cord malformations in genotyped cases and implications for neurodevelopmental functions of primary cilia. Acta Neuropathologica 123, 695–709. [PubMed: 22331178]

Kalil K, and Dent EW (2014). Branch management: mechanisms of axon branching in the developing vertebrate CNS. Nature Reviews Neuroscience 15, 7–18.. [PubMed: 24356070]

Katsura Y, Kubota H, Kunida K, Kanno A, Kuroda S, and Ozawa T (2015). An optogenetic system for interrogating the temporal dynamics of Akt. Scientific reports, 1–10.

Kholodenko BN (2006). Cell-signalling dynamics in time and space. Nature Reviews Molecular Cell Biology 7, 165–176. [PubMed: 16482094]

Klapoetke NC, Murata Y, Kim SS, Pulver SR, Birdsey-Benson A, Cho YK, Morimoto TK, Chuong AS, Carpenter EJ, Tian Z, et al. (2014). Independent optical excitation of distinct neural populations. Nature Methods 11, 338–346. [PubMed: 24509633]

Kwon C-H, Luikart BW, Powell CM, Zhou J, Matheny SA, Zhang W, Li Y, Baker SJ, and Parada LF (2006). Pten regulates neuronal arborization and social interaction in mice. Neuron 50, 377–388. [PubMed: 16675393]

Mariani LE, Ivanova AA, Suciu SK, Kahn RA, and Caspary T (2016). Arl13b regulates Shh signaling from both inside and outside the cilium. Mol Biol Cell 27, 3780–3790.

Lemmon MA, and Schlessinger J (2010). Cell Signaling by Receptor Tyrosine Kinases. Cell 141, 1117–1134. [PubMed: 20602996]

Madisen L, Zwingman TA, Sunkin SM, Oh SW, Zariwala HA, Gu H, Ng LL, Palmiter RD, Hawrylycz MJ, Jones AR, et al. (2010). A robust and high-throughput Cre reporting and characterization system for the whole mouse brain. Nature neuroscience 13, 133–140. [PubMed: 20023653]

Manning BD, and Cantley LC (2007). AKT/PKB Signaling: Navigating Downstream. Cell 129, 1261–1274. [PubMed: 17604717]

Manning BD, and Toker A (2017). AKT/PKB Signaling: Navigating the Network. Cell 169, 381–405. [PubMed: 28431241]

Marley A, and von Zastrow M (2012). A simple cell-based assay reveals that diverse neuropsychiatric risk genes converge on primary cilia. PLOS ONE 7, e46647. [PubMed: 23056384]

Mattila PK, and Lappalainen P (2008). Filopodia: molecular architecture and cellular functions. Nature Reviews Molecular Cell Biology 9, 446–454. [PubMed: 18464790]

McIntyre JC, Davis EE, Joiner A, Williams CL, Tsai I-C, Jenkins PM, McEwen DP, Zhang L, Escobado J, Thomas S, et al. (2012). Gene therapy rescues cilia defects and restores olfactory function in a mammalian ciliopathy model. Nature Medicine 18, 1423–1428.

Mejillano MR, Kojima S, Applewhite DA, Gertler FB, Svitkina TM, and Borisy GG (2004). Lamellipodial versus filopodial mode of the actin nanomachinery: pivotal role of the filament barbed end. Cell 118, 363–373. [PubMed: 15294161]

Miertzschke M, Koerner C, Spoerner M, and Wittinghofer A (2014). Structural insights into the small G-protein Arl13B and implications for Joubert syndrome. Biochem J. 457, 301–11. [PubMed: 24168557]

Mukhopadhyay S, and Rohatgi R (2014). G-protein-coupled receptors, Hedgehog signaling and primary cilia. Seminars in Cell and Developmental Biology 33, 63–72. [PubMed: 24845016]

Nachury MV, Seeley ES, and Jin H (2010). Trafficking to the ciliary membrane: how to get across the periciliary diffusion barrier? Annual Review of Cell and Developmental Biology 26, 59–87.

Nguyen T, and Di Giovanni S (2008). NFAT signaling in neural development and axon growth. Int J Dev Neurosci. 26, 141–145. [PubMed: 18093786]

Nichols AS, Floyd DH, Bruinsma SP, Narzinski K, and Baranski TJ (2013). Frizzled receptors signal through G proteins. Cellular Signalling 25, 1468–1475. [PubMed: 23524329]

Nishikimi M, Oishi K, and Nakajima K (2013). Axon Guidance Mechanisms for Establishment of Callosal Connections. Neural Plasticity 2013, 1–7.

Novarino G, Akizu N, and Gleeson JG (2011). Modeling Human Disease in Humans: The Ciliopathies. Cell 147, 70–79. [PubMed: 21962508]

Omori Y, Chaya T, Yoshida S, Irie S, Tsujii T, and Furukawa T (2015). Identification of G Protein-Coupled Receptors (GPCRs) in Primary Cilia and Their Possible Involvement in Body Weight Control. PLOS ONE 10, e0128422–0128417. [PubMed: 26053317]

Oude Weernink PA, Han L, Jakobs KH, and Schmidt M (2007). Dynamic phospholipid signaling by G protein-coupled receptors. Biochimica et Biophysica Acta (BBA) - Biomembranes 1768, 888–900. [PubMed: 17054901]

Parisi MA (2019). The molecular genetics of Joubert syndrome and related ciliopathies: The challenges of genetic and phenotypic heterogeneity. Translational Science of Rare Diseases 4, 25–49. [PubMed: 31763177]

Parra LM, and Zou Y (2010). Sonic hedgehog induces response of commissural axons to Semaphorin repulsion during midline crossing. Nature neuroscience 13, 29–35. [PubMed: 19946319]

Patro R, Duggal G, Love MI, Irizarry RA, and Kingsford C (2017). Salmon provides fast and bias-aware quantification of transcript expression. Nature Methods 14, 417–419. [PubMed: 28263959]

Paxinos G, and Franklin KBJ (2001). The Mouse Brain in Stereotaxic Coordinates, Academic Press.

Phua SC, Chiba S, Suzuki M, Su E, Roberson EC, Pusapati GV, Setou M, Rohatgi R, Reiter JF, Ikegami K, et al. (2017). Dynamic Remodeling of Membrane Composition Drives Cell Cycle through Primary Cilia Excision. Cell 168, 264–279.e215. [PubMed: 28086093]

Phua SC, Lin Y-C, and Inoue T (2015). An intelligent nano-antenna: Primary cilium harnesses TRP channels to decode polymodal stimuli. Cell Calcium 58, 415–422. [PubMed: 25828566]

Plotnikova OV, Seo S, Cottle DL, Conduit S, Hakim S, Dyson JM, Mitchell CA, and Smyth IM (2015). INPP5E interacts with AURKA, linking phosphoinositide signaling to primary cilium stability. J Cell Sci. 128, 364–72. [PubMed: 25395580]

Poretti A, Boltshauser E, Loenneker T, Valente EM, Brancati F, Il'yasov K, and Huisman TAGM (2007). Diffusion tensor imaging in Joubert syndrome. AJNR American journal of neuroradiology 28, 1929–1933. [PubMed: 17898198]

Puram SV, Kim AH, Ikeuchi Y, Wilson-Grady JT, Merdes A, Gygi SP, and Bonni A (2011). A CaMKIIbeta signaling pathway at the centrosome regulates dendrite patterning in the brain. Nat Neurosci 14, 973–983. [PubMed: 21725312]

Rafiullah R, Long AB, Ivanova AA, Ali H, Berkel S, Mustafa G, Paramasivam N, Schlesner M, Wiemann S, Wade RC, et al. (2017). A novel homozygous ARL13B variant in patients with Joubert syndrome impairs its guanine nucleotide-exchange factor activity. European Journal of Human Genetics 25, 1324–1334. [PubMed: 29255182]

Raper J, and Mason C (2010). Cellular Strategies of Axonal Pathfinding. Cold Spring Harbor Perspectives in Biology 2, a001933–a001933. [PubMed: 20591992]

Reiter JF, and Leroux MR (2017). Genes and molecular pathways underpinning ciliopathies. Nat Rev Mol Cell Biol 18, 533–547. [PubMed: 28698599]

Romani M, Micalizzi A, and Valente EM (2013). Joubert syndrome: congenital cerebellar ataxia with the molar tooth. The Lancet Neurology 12, 894–905. [PubMed: 23870701]

Sánchez-Alegría K, Flores-León M, Avila-Muñoz E, Rodríguez-Corona N, and Arias C (2018). PI3K Signaling in Neurons: A Central Node for the Control of Multiple Functions. Int J Mol Sci. 23, 19.

Sarkisian MR, and Guadiana SM (2015). Influences of Primary Cilia on Cortical Morphogenesis and Neuronal Subtype Maturation. The Neuroscientist 21, 136–151. [PubMed: 24740576]

Sattar S, and Gleeson JG (2011). The ciliopathies in neuronal development: a clinical approach to investigation of Joubert syndrome and Joubert syndrome-related disorders. Developmental Medicine & Child Neurology 53, 793–798. [PubMed: 21679365]

Sawano A, Takayama S, Matsuda M, and Miyawaki A (2002). Lateral Propagation of EGF Signaling after Local Stimulation Is Dependent on Receptor Density. Developmental Cell 3, 245–257. [PubMed: 12194855]

Schmid RS, McGrath B, Berechid BE, Boyles B, Marchionni M, Sestan N, and Anton ES (2003). Neuregulin 1-erbB2 signaling is required for the establishment of radial glia and their transformation into astrocytes in cerebral cortex. Proc Natl Acad Sci U S A 100, 4251–4256. [PubMed: 12649319]

Schou KB, Pedersen LB, and Christensen ST (2015). Ins and outs of GPCR signaling in primary cilia. EMBO reports 16, 1099–1113. [PubMed: 26297609]

Senocak EU, Oguz KK, Haliloglu G, Topcu M, and Cila A (2010). Structural abnormalities of the brain other than molar tooth sign in Joubert syndrome-related disorders. Diagn Interv Radiol 16, 3–6. [PubMed: 20108204]

Spangler SM, and Bruchas MR (2017). Optogenetic approaches for dissecting neuromodulation and GPCR signaling in neural circuits. Current opinion in pharmacology 32, 56–70. [PubMed: 27875804]

Stierl M, Stumpf P, Udwari D, Gueta R, Hagedorn R, Losi A, Gartner W, Petereit L, Efetova M, Schwarzel M, et al. (2011). Light modulation of cellular cAMP by a small bacterial photoactivated adenylyl cyclase, bPAC, of the soil bacterium Beggiatoa. J Biol Chem 286, 1181–1188. [PubMed: 21030594]

Su C-Y, Bay SN, Mariani LE, Hillman MJ, and Caspary T (2012). Temporal deletion of Arl13b reveals that a mispatterned neural tube corrects cell fate over time. Development (Cambridge, England) 139, 4062–4071.

Su S, Phua SC, DeRose R, Chiba S, Narita K, Kalugin PN, Katada T, Kontani K, Takeda S, and Inoue T (2013). Genetically encoded calcium indicator illuminates calcium dynamics in primary cilia. Nature Methods 10, 1105–1107. [PubMed: 24056873]

Thomas S, Cantagrel V, Mariani L, Serre V, Lee J-E, Elkhartoufi N, de Lonlay P, Desguerre I, Munnich A, Boddaert N, et al. (2015). Identification of a novel ARL13B variant in a Joubert syndrome-affected patient with retinal impairment and obesity. European journal of human genetics : EJHG 23, 621–627. [PubMed: 25138100]

Umberger NL, and Caspary T (2015). Ciliary transport regulates PDGF-AA/αα signaling via elevated mammalian target of rapamycin signaling and diminished PP2A activity. Molecular Biology of the Cell 26, 350–358. [PubMed: 25392303]

Vitriol EA, and Zheng JQ (2012). Growth cone travel in space and time: the cellular ensemble of cytoskeleton, adhesion, and membrane. Neuron 73, 1068–1081. [PubMed: 22445336]

Wang L, and Marquardt T (2013). What axons tell each other: axon-axon signaling in nerve and circuit assembly. Curr Opin Neurobiol 23, 974–982. [PubMed: 23973157]

Wang Z, Zhou Y, Luo Y, Zhang J, Zhai Y, Yang D, Zhang Z, Li Y, Storm D, and Ma R (2015). Gene Expression Profiles of Main Olfactory Epithelium in Adenylyl Cyclase 3 Knockout Mice. International Journal of Molecular Sciences 16, 28320–28333. [PubMed: 26633363]

Weimer JM, Stanco A, Cheng J-G, Vargo AC, Voora S, and Anton ES (2008). A BAC transgenic mouse model to analyze the function of astroglial SPARCL1 (SC1) in the central nervous system. Glia 56, 935–941. [PubMed: 18381651]

Welf ES, Ahmed S, Johnson HE, Melvin AT, and Haugh JM (2012). Migrating fibroblasts reorient directionality by a metastable, PI3K-dependent mechanism. The Journal of Cell Biology 197, 105–114. [PubMed: 22472441]

Winkle CC, Taylor KL, Dent EW, Gallo G, Greif KF, and Gupton SL (2016). Beyond the cytoskeleton: The emerging role of organelles and membrane remodeling in the regulation of axon collateral branches. Developmental Neurobiology 76, 1293–1307. [PubMed: 27112549]

Yokota Y, Ring C, Cheung R, Pevny L, and Anton ES (2007). Nap1-Regulated Neuronal Cytoskeletal Dynamics Is Essential for the Final Differentiation of Neurons in Cerebral Cortex. Neuron 54, 429–445. [PubMed: 17481396]

Yu TW, and Bargmann CI (2001). Dynamic regulation of axon guidance. Nature neuroscience 4, 1169–1176.

Zhu D, Shi S, Wang H, and Liao K (2009). Growth arrest induces primary-cilium formation and sensitizes IGF-1-receptor signaling during differentiation induction of 3T3-L1 preadipocytes. Journal of Cell Science 122, 2760–2768. [PubMed: 19596798]

Highlights

- Chemogenetic and or optogenetic activation of primary cilia alters axonal behavior.
- Ciliary activity modulates axonal growth cones and filopodial/lamellipodial balance.
- Arl13b-Inpp5e activity in cilia facilitates axonal tract formation and targeting.
- Disrupted ciliary signaling contributes to axonal tract malformations in JSRD.

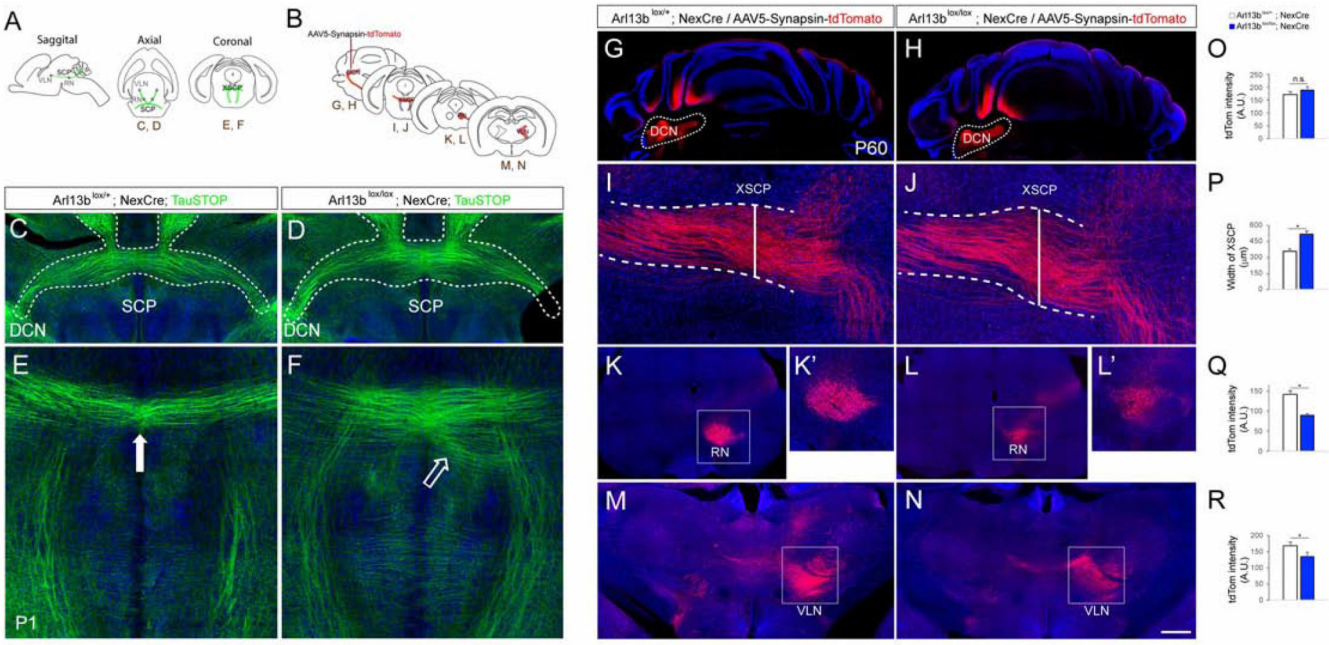

Figure 1. Deletion of *Arl13b* leads to SCP axonal tract defects.

(A) Schematic of SCP tract in sagittal (left), axial (middle), and coronal (right) sections. (B) Schematic of SCP axonal projection labeling by unilateral injection of AAV5-Synapsin-tdTom into the DCN. (C-D) GFP labeling shows "x" shaped SCP tract (outlined in white dashed line) in *Arl13b*$^{lox/+}$*; NexCre; Taustop* (C) and *Arl13b*$^{lox/lox}$*; NexCre; Taustop* (D) axial sections. (E, F) GFP labeling show SCP tract in *Arl13b*$^{lox/+}$*; NexCre; Taustop* (E) and *Arl13b*$^{lox/lox}$*; NexCre; Taustop* (F) in coronal sections (P1). White arrow (E) points to SCP decussation in control. Arrow (F) points to diffused, misoriented axons of SCP in *Arl13b*$^{lox/lox}$*; NexCre; Taustop* brains. (G, H) Coronal cerebellar sections show tdTom^{+} DCN neurons in *Arl13b*$^{lox/+}$*; NexCre* (G) and *Arl13b*$^{lox/lox}$*; NexCre* (H) brains (P60). DCN is outlined with dotted lines. (I, J) tdTom^{+} SCP decussation is wider in mutants. White dashed lines outline the width of SCP tract. (K, L) tdTom^{+} SCP axons innervate the RN. (K', L') Higher magnification of the RN region (white box) in K and L. (M, N) The target projection pattern of SCP into VLN of the thalamus. (O) Quantification of tdTom fluorescence intensity in the DCN indicates no significant differences. (P) Quantification of XSCP width. (Q, R) Quantification of fluorescence density of tdTom^{+} DCN axonal terminals in RN (Q) and VLN (R) indicates reduced projection in Arl13b cKO brains. Data shown are mean±SEM (n=4 brains per group). *P<0.05 (Student's t-test). DCN, deep cerebellar nuclei; SCP, superior cerebellar peduncle; RN, red nucleus; VLN, ventrolateral nucleus; XSCP, decussation of SCP. Scale bar, 425μm (C, D); 142μm (G, H), 238μm (I, J), 832μm (K, L), 960μm (M, N). See also SFig. 3.

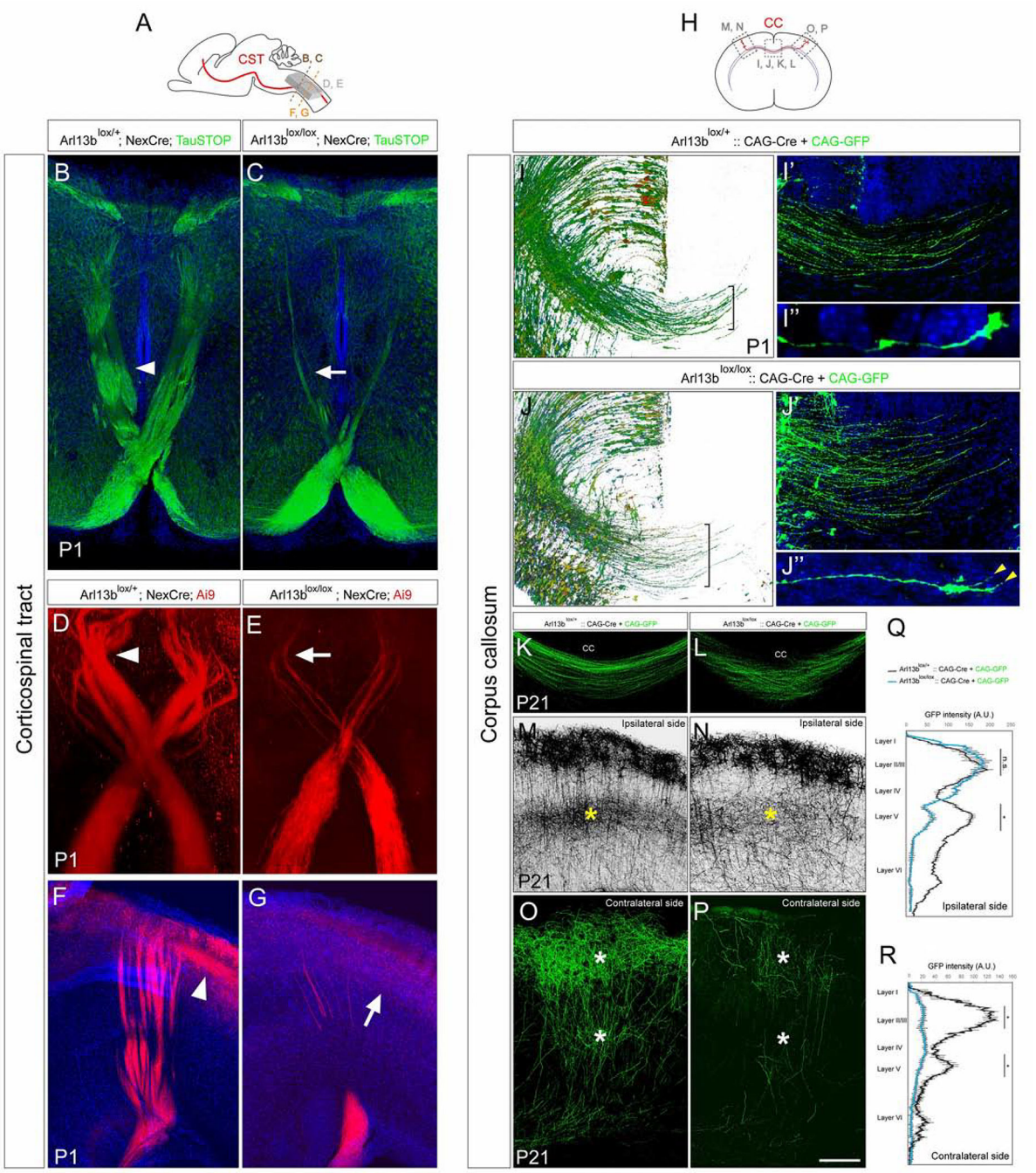

Figure 2. Deletion of *Arl13b* leads to CST and CC axonal tracts defects.

(A) Schematic of CST tract in sagittal section. Dashed lines indicate where the CST decussation is and where B-C and F-G were imaged, respectively. Gray box indicates where D and E were imaged in cleared brains. (B, C) GFP^{+} CST tract decussation at lower medulla of *Arl13b$^{lox/+}$; NexCre; Taustop* (B, arrowhead) and *Arl13b$^{lox/lox}$; NexCre; Taustop* (C, arrow) brains (P1). (D, E) CST decussation in cleared *Arl13b$^{lox/+}$; NexCre; Ai9* (D) and *Arl13b$^{lox/lox}$; NexCre; Ai9* (E) brains. Arrowhead (D) and arrow (E) point to the CST fascicles post decussation. (F, G) Sagittal sections of *Arl13b$^{lox/+}$; NexCre; Ai9* (F) and

Arl13b$^{lox/lox}$*; NexCre; Ai9* (G) (P1) show reduced tdTom^{+} CST tract fascicles post decussation and the reduced extension of CST axons into the dorsal spinal cord in mutants (G [arrow]; compare to control [F, arrowhead]). (H) Schematic of CC tract in coronal section. Dashed rectangles indicate where I-P were imaged. (I, J) *Arl13b*$^{lox/+}$ (I) and *Arl13b*$^{lox/lox}$ (J) embryos (E15) were electroporated with pCAG-Cre and pCAG-GFP plasmids. GFP labeled callosal axons in CC were analyzed at P1. Brackets indicate the width of CC. (I', J') CC area highlighted in I and J. (I", J") Representative GFP^{+} axonal growth cone of callosal neurons at the midline. Arrowheads point to longer filopodia in mutants. (K-P) pCAG-Cre and pCAG-GFP electroporated *Arl13b*$^{lox/+}$ (K, M, O) and *Arl13b*$^{lox/lox}$ (L, N, P) embryos (E15) were analyzed at P21. GFP labeling show disorganized CC axons in *Arl13b*$^{lox/lox}$ brains (L) electroporated with pCAG-Cre when compared to control (K). (M-P) Reduced axonal branching is evident in ipsilateral layer 5 (yellow asterisk, M, N) and contralateral layers 2/3 and 5 (white asterisks, O, P) in *Arl13b*$^{lox/lox}$; Cre brains. (Q, R) Quantification of GFP fluorescence intensity in the ipsilateral (Q) and contralateral (R) cortical wall. Data shown are mean±SEM (n=4 brains per group). *P<0.05 (Student's t-test). Scale bar, 135μm (B-G); 95μm (I, J); 1200μm (K, L); 415μm (M, N); 623μm (O, P).

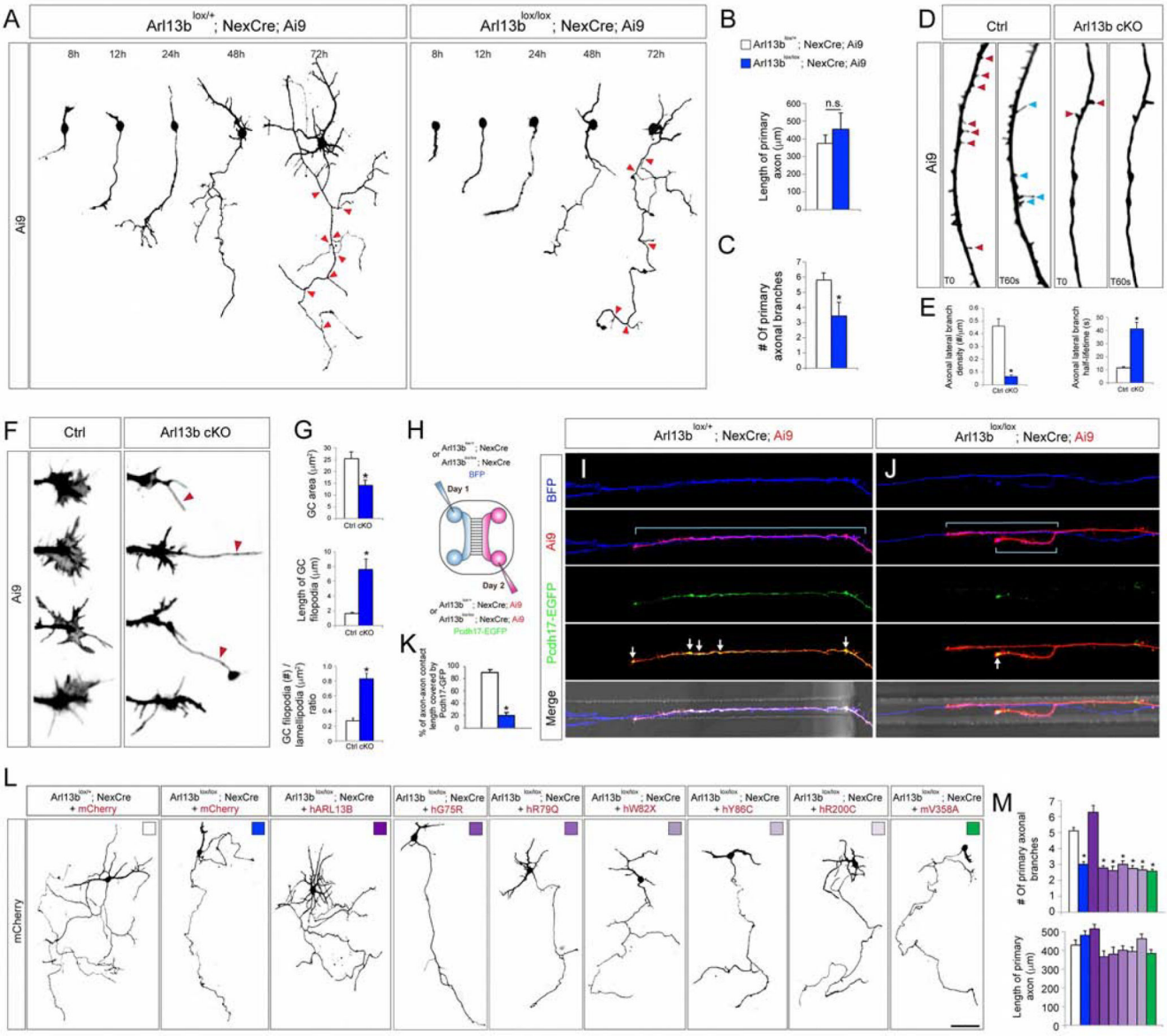

Figure 3. Deletion of *Arl13b* leads to axonal growth defects *in vitro*.

(A) Growth of DCN neurons dissociated from *Arl13b*$^{lox/+}$*; NexCre; Ai9* and *Arl13b*$^{lox/lox}$*; NexCre; Ai9* (cKO) brains (P2) were analyzed at different time points as indicated. Red arrowheads point to the primary axonal branching points. (B, C) Quantification of axonal outgrowth at 3 days *in vitro* (DIV). Data shown are mean±SEM (n=24 neurons). **P*<0.05 (Student's *t*-test). (D) Axonal filopodia dynamics of DCN neurons from *Arl13b*$^{lox/+}$*; NexCre; Ai9* (Ctrl) and *Arl13b*$^{lox/lox}$*; NexCre; Ai9* (Arl13b cKO) brains. Red arrowheads point to representative axonal filopodia at time 0sec. Blue arrowheads point to newly formed axonal filopodia at time 60sec. (E) Quantification of axonal lateral branch density and half lifetime. Data shown are mean±SEM (n=24 neurons). **P*<0.05 (Student's *t*-test). (F) Representative axonal growth cones of DCN neurons from Ctrl and Arl13b cKO brains. Red arrowheads point to aberrantly long filopodia extensions. (G) Quantification of axonal

growth cone (GC) area, axonal filopodia length, and growth cone filopodia/lamellipodia ratio. Data shown are mean±SEM (n=28 cells). **P*<0.05 (Student's *t*-test). (H) Schematic of the microfluidic chamber assay for the expression of Pcdh17-EGFP along axon-axon contacts. (I, J) Expression of Pcdh17-GFP along the $BFP^+/tdTom^+$ axon-axon contact sites in DCN neurons of Ctrl (I) and Arl13b cKO (J) brains. White brackets indicate $BFP^+/tdTom^+$ axon-axon contact regions. White arrows point to Pcdh17 expression at axon-axon contact sites. (K) Quantification of Pcdh17-$EGFP^+$ axon-axon contacts. (L) Effect of human ARL13B mutations on axon growth. DCN neurons of *Arl13b*$^{lox/+}$*; NexCre* and *Arl13b*$^{lox/lox}$*; NexCre* were transfected with mCherry, mCherry-ARL13B (wild type or different human mutations), or mV358A mutant and analyzed after 3 days. (M) Quantification of primary axonal length and branch number. Data shown are mean±SEM. **P*<0.05 (One-way ANOVA: $F_{8,216}$ =24.11; p=4.7E-33; post-hoc $p_{[lox/+ \text{ vs. } lox/lox}$=6.0E-14; post-hoc $p_{[lox/+ \text{ vs. } lox/lox\text{-}ARL13B}$=0.09; post-hoc $p_{[lox/+ \text{ vs. } lox/lox\text{-}G75R]}$=5.6E-10; post-hoc $p_{[lox/+ \text{ vs. } lox/lox\text{-}R79Q]}$=6.8E-09; post-hoc $p_{[lox/+ \text{ vs. } lox/lox\text{-}W82X]}$=9.5E-09; post-hoc $p_{[lox/+ \text{ vs. } lox/lox\text{-}Y86C]}$=4.8E-10; post-hoc $p_{[lox/+ \text{ vs. } lox/lox\text{-}R200C]}$=2.1E-10; post-hoc $p_{[lox/+ \text{ vs. } lox/lox\text{-}V358A]}$=2.5E-11; 25 neurons). Scale bar, 28μm (A), 8μm (D, F), 4.5μm (J, K), 30μm (L). See also SFig. 5.

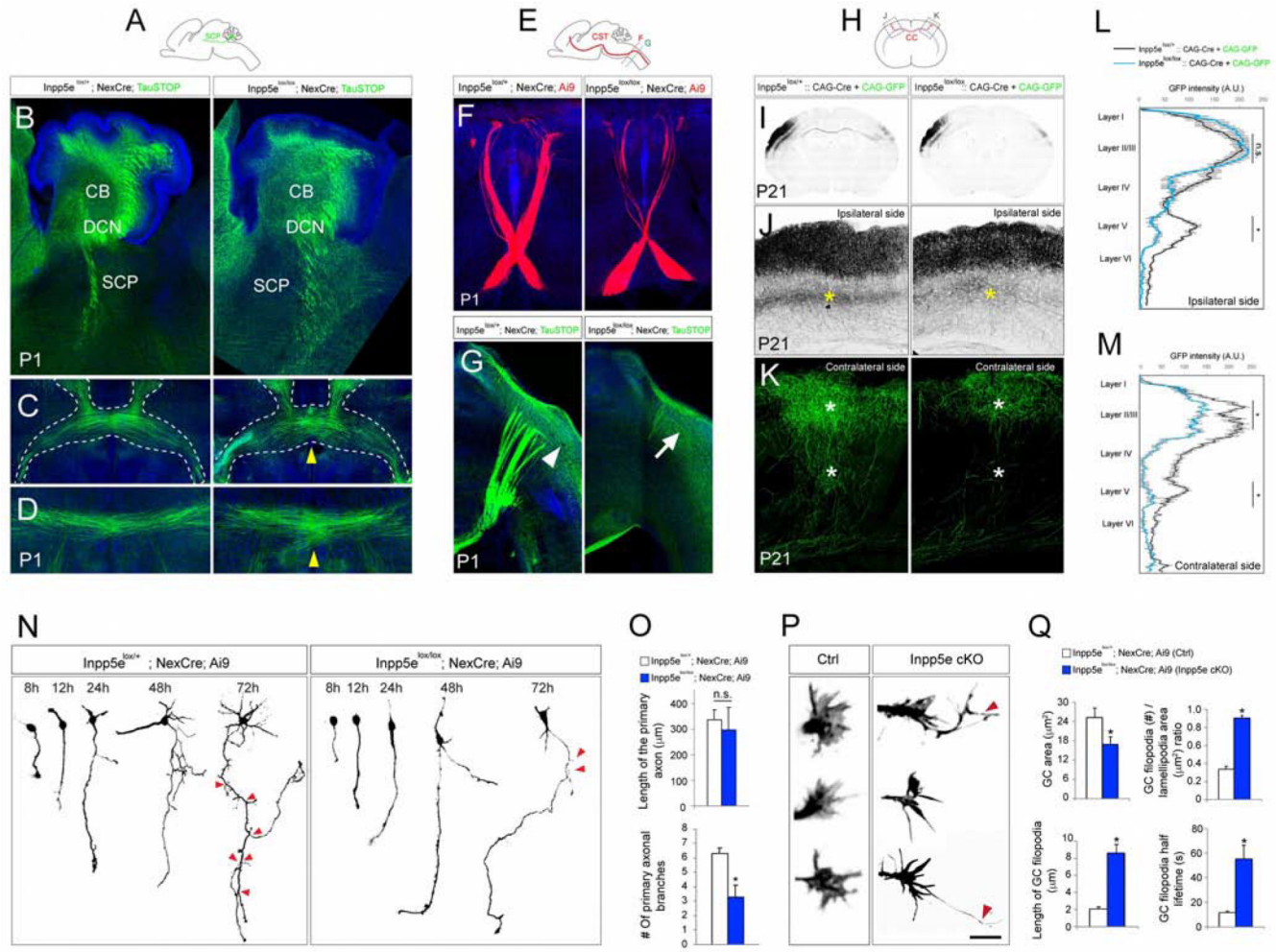

Figure 4. Deletion of *Inpp5e* leads to axonal defects similar to Arl13b cKO.

(A) Schematic of SCP tract in sagittal sections. (B- D) GFP labeling in *Inpp5e*$^{lox/+}$*; NexCre; Taustop* and *Inpp5e*$^{lox/lox}$*; NexCre; Taustop* brains (P1) show the trajectory of SCP tract in sagittal (B), axial (C), and coronal (D) sections. (B) Diffused outgrowth of SCP in Inpp5e cKO when compared to control. Dashed lines (C) outline the SCP decussation in axial sections. Yellow arrowheads in C and D point to the diffused, wider, and disrupted decussation of SCP in Inpp5e mutants. (E) Schematic of CST tract in sagittal sections. Dashed lines indicate where F and G were imaged, respectively. (F) Altered decussation of TdTom^{+} CST in *Inpp5e*$^{lox/lox}$*; NexCre; Ai9* brains. (G) Reduced GFP^{+} CST tract fascicles post decussation and reduced extension of CST axons into the dorsal spinal cord in mutants (arrow; compare to control [arrowhead]). (H) Schematic of CC tract in coronal sections. Outlined areas indicate where J and K were imaged. (I-K) *Inpp5e*$^{lox/+}$ and *Inpp5e*$^{lox/lox}$ embryos (E15) were electroporated with pCAG-Cre and pCAG-GFP plasmids and analyzed at P21. (I) Low magnification images of GFP labeled CC tract. (J-K) Reduced axonal branching is evident in ipsilateral layer 5 (yellow asterisk) and contralateral layers 2/3 and 5 (white asterisks) in *Inpp5e*$^{lox/lox}$ brains electroporated with pCAG-Cre. (L-M) Quantification of GFP fluorescence intensity (arbitrary units) along the cortical wall of ipsilateral side (L) and contralateral side (M). Data shown are mean±SEM (n=4 brains). *P<0.05 (Student's t-

test). (N) Dissociated DCN neurons from *Inpp5e*$^{lox/+}$*; NexCre; Ai9* (Ctrl) and *Inpp5e*$^{lox/lox}$*; NexCre; Ai9* (Inpp5e cKO) brains were analyzed at different time points as indicated. Red arrowheads point to the primary axonal branching points. (O) Quantification of axonal outgrowth (3 DIV). Data shown are mean±SEM (n=24 neurons). **P*<0.05 (Student's *t*-test). (P) Representative axonal growth cones of DCN neurons from Ctrl and Inpp5e cKO brains. Red arrowheads point to aberrantly long filopodial extensions. (Q) Quantification of axonal growth cone area, filopodia length, filopodial half lifetime, and growth cone filopodia/lamellipodia ratio. Data shown are mean±SEM (n=24 cells). **P*<0.05 (Student's *t*-test). CB, cerebellum; DCN, deep cerebellar nuclei; SCP, superior cerebellar peduncle; GC, growth cone. Scale bar, 205μm (B), 150μm (C, D), 600μm (F, G), 1215μm (I), 240μm (J), 340μm (K), 25μm (N), 5μm (P).

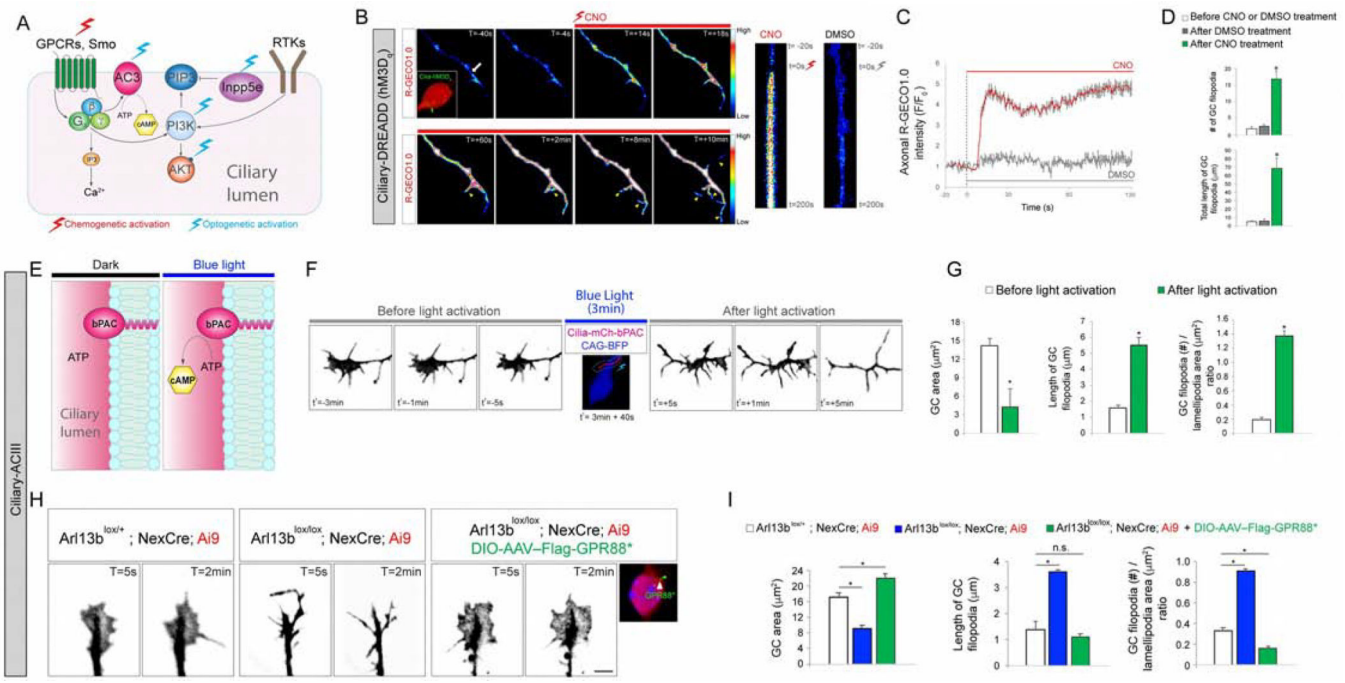

Figure 5. Chemogenetic or optogenetic manipulation of ciliary GPCR signaling leads to rapid changes in axonal growth cone dynamics.

(A) Schematic depicting optogenetic/chemogenetic approaches to manipulate different inter-related ciliary signaling pathways (GPCRs, ACIII, PI3K, AKT, Inpp5e). (B) Time-lapse imaging of control DCN neuron axon expressing Cilia-hM3D$_q$ and RFP-GECO1.0 (pseudocolored) treated with 10μM CNO (left panel). Yellow arrowheads point to the filopodial extensions. Kymograph of the changes in RFP-GECO1.0 fluorescence intensity at the distal axonal tip (white arrow at T0) upon CNO or DMSO treatment. (C) Axonal RFP-GECO1.0 fluorescence intensity before and after CNO or DMSO treatment (n=16 cells). Data shown is mean±SEM. Relative intensity of RFP (F/F$_0$) at peak [CNO vs. DMSO]: p= 1.2E-8, Student's *t*-test. (D) Quantification of changes in the growth cone morphology before and after CNO or DMSO treatment. Data shown are mean±SEM (n=24 neurons). *P<0.05 (Student's *t*-test). (E) Schematic of bPAC mediated, blue light-dependent cAMP production in primary cilia. (F, G) Changes in the growth cone morphology before and after ciliary activation of bPAC in control DCN neurons expressing Cilia-bPAC and pCAG-BFP. t' in panel F includes 20 seconds to move from growth cone (pre-light activation) to primary cilia, blue light photo-activation of primary cilia (3 mins.) and 20 seconds to move back to growth cone (post-light activation). Data shown are mean± SEM (n=24 neurons). *P<0.05 (Student's *t*-test). (H) Inhibition of ciliary ACIII activity with modified GPR88* in Arl13b-deficient neurons. Live imaging of growth cone dynamics in *Arl13b$^{lox/+}$; NexCre; Ai9*, *Arl13b$^{lox/lox}$; NexCre; Ai9, and Arl13b$^{lox/lox}$; NexCre; Ai9+* DIO-AAV-Flag-GPR88* DCN neurons. Inset shows expression of FLAG tagged GPR88* in cilium. (I) Quantification of growth cone (GC) morphology. Data shown are mean±SEM. *P<0.05 (One-way ANOVA: $F_{2,42[\text{GC area}]}$ =32.0; p=3.6E-9; post-hoc $p_{[\text{GC area, lox/+ vs. lox/lox}]}$= 6.9E-06; post-hoc $p_{[\text{GC area, lox/+ vs. lox/lox-GPR88*}]}$=0.01; $F_{2,42[\text{\# of GC filopodia}]}$=36.6; p=6.2E-10; post-hoc $p_{[\text{\# of filopodia, lox/+ vs. lox/lox}]}$=1.1E-04; post-hoc $p_{[\text{lox/+ vs. lox/lox-GPR88*}]}$=0.001;

$F_{2,42[\text{L of GC filopodia}]}$=50.4; p=6.9E-12; post-hoc $p_{[\text{L of GC filopodia, lox/+ vs. lox/lox}]}$=1.8E-07; post-hoc $p_{[\text{L of GC filopodia, lox/+ vs. lox/lox-GPR88}]}$=0.07; n=15 neurons). Scale bar, 4μm (B); 8.5μm (F, H).

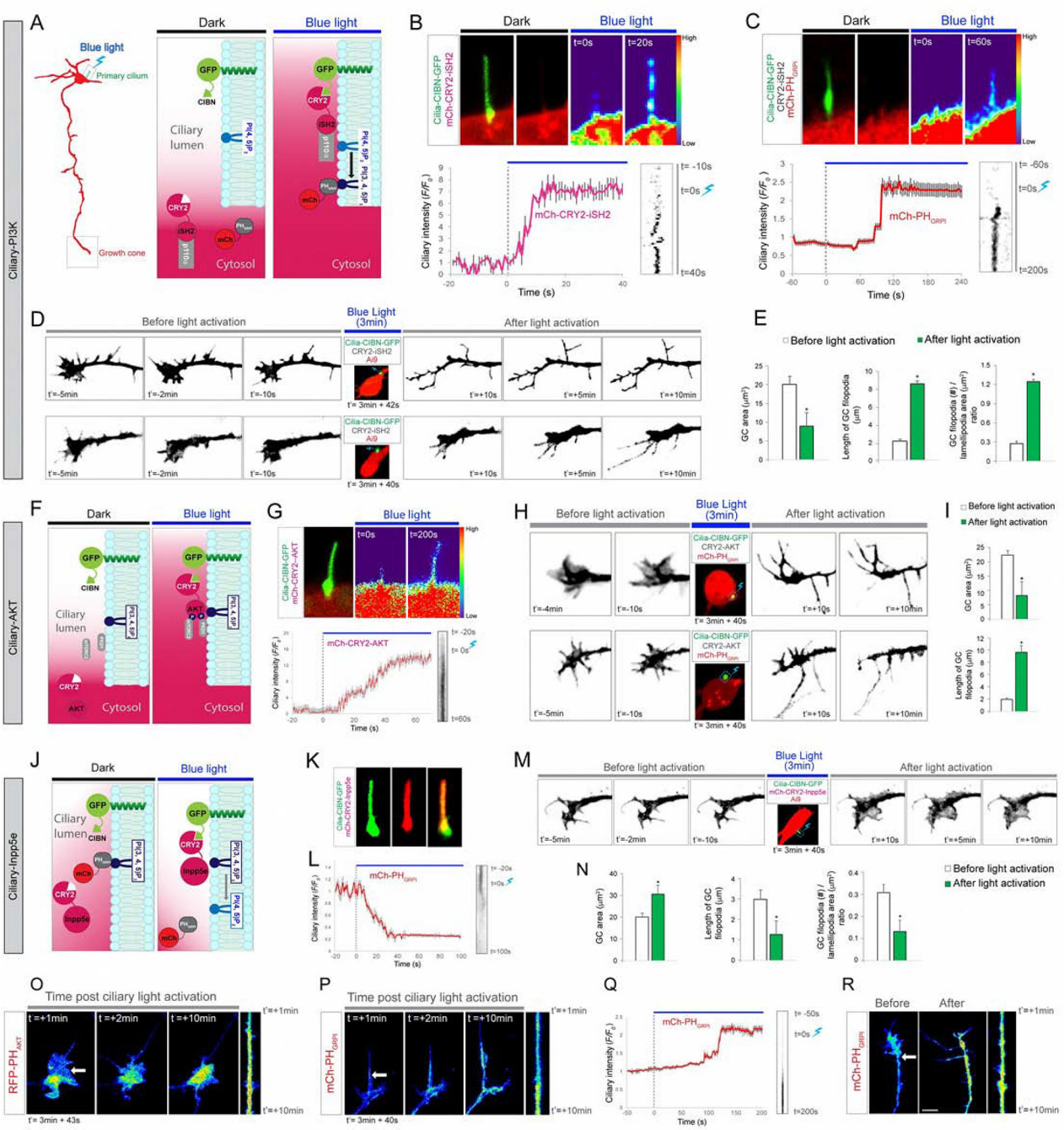

Figure 6. Optogenetic manipulation of ciliary PI3K/AKT signaling leads to rapid changes in axonal growth cone dynamics.

(A) Schematic of optogenetic recruitment of PI3-kinase to the cilium and evaluation of changes in axonal growth cone. Untagged (CRY2-iSH2) or mCherry tagged iSH2 (mCh-CRY2-iSH2) was used. PIP3 sensor mCh-PH_{GRPI} was not included in experiments where mCh-CRY2-iSH2 was used. (B-C) Expression of Cilia-CIBN-GFP and mCh-CRY2-iSH2 (B) or mCh-PH_{GRPI} (C) in the primary cilia of control DCN neurons before and after ciliary blue light activation (upper panels, B-C). Lower panels (B-C) illustrate the dynamics and kymographs of the ciliary mCh-CRY2-iSH2 (B) and mCh-PH_{GRPI} (C) intensity before and

after ciliary blue light illumination (n=16 cells). (D-E) Changes in the growth cone morphology before and after ciliary recruitment of PI3-kinase in two different DCN neurons expressing Cilia-CIBNGFP and CRY2-iSH2. Data shown are mean±SEM (n=24 neurons). *P<0.05 (Student's t-test). (F) Schematic of optogenetic recruitment of AKT to the ciliary membrane. (G) Expression of Cilia-CIBN-GFP and mCh-CRY2-AKT in the primary cilia of control DCN neurons before and after ciliary blue light activation (upper panels). Lower panels illustrate the dynamics and kymograph of ciliary mCh-CRY2-AKT intensity before and after ciliary blue light activation (n=16 cells). (H-I) Changes in the growth cone morphology before and after ciliary recruitment of AKT in two different DCN neurons expressing Cilia-CIBN-GFP and CRY2-AKT, and mCh-PH_{GRPI}. Data shown are mean ±SEM (n=24 neurons). *P<0.05 (Student's t-test). (J) Schematic of optogenetic recruitment of $5pase_{INPP5E}$ to the ciliary membrane. (K) Expression of Cilia-CIBN-GFP and mCh-CRY2–$5pase_{INPP5E}$ in the primary cilia of DCN neurons. (L) Dynamics and kymograph of PIP3 sensor mCh-PH_{GRPI} intensity in primary cilia after ciliary recruitment of $5pase_{INPP5E}$ (n=16 cells). (M-N) Changes in the growth cone morphology before and after ciliary recruitment of $5pase_{INPP5E}$ in DCN neurons expressing Cilia-CIBN-GFP and mCh-CRY2–$5pase_{INPP5E}$. Data shown are mean±SEM (n=24 neurons). *P<0.05 (Student's t-test). (O-P) Changes in fluorescence intensity of PIP3 reporters, RFP-PH_{AKT} (O) and mCh-PH_{GRPI} (P), in axonal growth cone (white arrow) after ciliary activation of PI3-kinase. (Q, R) Dynamics and kymograph of mCh-PH_{GRPI} intensity in primary cilia (Q) and axonal growth cone (R) after ciliary activation of AKT (n=16 cells). t' in panels D, H, M, O, P, R includes 20 seconds to move from growth cone (pre-light activation) to primary cilia, blue light photo-activation of primary cilia (3 mins.) and 20–23 seconds to move back to growth cone (post-light activation). Scale bar, 1.5μm (B, C, G, K, O, P, R); 2.5μm (D, H, M). See also SFig. 7.